

WM- /  
PDR  
(Return to WM, 623-SS)

See Pocket 2  
for ends

3109.1/FRC/82/07/01/0

NOV 8 1982

Distribution: w/o encl.  
WM file  
WMHL r/f  
NMSS r/f  
JBMartin  
REBrowning  
MJBell  
FRCook & r/f  
HJMiller  
JOBunting  
PDR

Mr. Wade Ballard, Jr.  
Acting Director  
Division of Waste Repository Deployment  
Office of Waste Isolation  
U. S. Department of Energy  
Washington, DC 20545

Dear Mr. Ballard:

The attached Brookhaven National Laboratory reports prepared under contract to NRC identify phenomena potentially applicable to assessing long term performance of high-level waste packages constructed of TiCode-12 alloy. These phenomena include crevice corrosion and hydrogen embrittlement.

The reports also provide data which point out the importance of the radiation environment, which could result in generation of hydrogen gas, in contributing to hydrogen pickup in TiCode-12.

These reports are provided in the interest of ensuring DOE's ongoing programs for selecting waste package designs and assessing long term performance of these designs under anticipated repository conditions will take these phenomena into account.

In accordance with your letter of July 1, 1982 to Mr. Martin I am sending copies of this letter and its enclosures to the respective project officers for the basalt, tuff and salt repositories.

Sincerely,

*MJB*

Michael J. Bell, Chief  
High-Level Waste Licensing  
Management Branch  
Division of Waste Management

Enclosures: BNL Quarterly Reports:  
BNL-NUREG-51499, Vol. 1, No. 3; Vol. 1,  
No. 4 and Vol. 2, No. 1.

cc: Donald Vieth  
Jeff Neff  
John Antonin  
Donald Schweitzer

8212020199 821108

PDR WASTE  
WM-1

PDR

OFC :	WMHL	:	WMHL	:	WM	:		:	
NAME :	FRCook: lmc	:	MJBell	:	REBrowning	:	JB Martin	:	
DATE :	11/ /82	:	11/ /82	:	11/3 /82	:	11/ /82	:	

3109.1/FRC/82/07/01/0

- 2 -

NOV 8 1982

bcc: M. Steindler  
H. Miller  
J. Davis

OFC	: WMHL <i>AKL</i>	: WMHL <i>MS</i>	: WM <i>RB</i>	: WM <i>AKL</i>	:	:	:
NAME	: FRCook: lmc	: MJBell	: REBrowning	: JB Martin	:	:	:
DATE	: 11/2/82	: 11/8/82	: 11/03/82	: 11/4/82	:	:	:

3109.1/FRC/82/07/01/0

- 1 -

DISTRIBUTION

WMHL file  
WMHL r/f  
WM r/f  
NMSS r/f  
JB Martin  
RE Browning  
MJ Bell  
HJ Miller  
JO Bunting  
FR Cook & r/f

WMHL: 3109.1

Mr. Wade Ballard  
Office of Waste Isolation  
U. S. Department of Energy  
Washington, DC 20545

Dear Mr. Ballard:

The attached Brookhaven National Laboratory report prepared under contract to NRC identifies evidence of several potential failure modes in the TiCode 12 now being considered as a candidate for high level waste package material. These failure modes include:

- a. Crevice Corrosion
- b. Stress Corrosion Cracking
- c. Hydrogen Embrittlement

The report notes how a radiation environment complicates the understanding of the mechanisms involved in each of these failure modes. Hydrogen generation is of particular concern in this regard.

These failure modes are likely to be major licensing issues if a package design is proposed that incorporates this alloy as a canister or overpack material. I urge that DOE aggressively investigate these failure modes in TiCode 12 such that a quantitative understanding of the degradation by these modes, supported by qualifying data obtained using agreed upon test methods, is available at licensing, if TiCode 12 is selected as a waste package material.

We would be pleased to participate in meetings with the cognizant DOE contractors to further detail our concerns in the context of their ongoing investigations for each of the repository projects. We note such a meeting is already being planned with the BWIP project for August 1982. Other meetings like the Research and Design Interface Meeting at Sandia National Laboratory in March would also provide a valuable opportunity to exchange information.

---

OFC	:	WMHL	<i>ALL</i>	:	WMHL	:	WM	:	<i>MS</i>	:	:	:
NAME	:	FRCook: lmc	:	MJBe11	:	REBrowning	<i>REB</i>	:	<i>JB Martin</i>	:	:	:
DATE	:	7/16/82	:	7/1/82	:	7/17/82	:	:	:	:	:	:

---

109.1

Encls to  
11-8-82 Hrt

**DRAFT**

DOE NUREG/CR-2317  
BNL-NUREG-51449  
Vol. 1, No. 4  
AN, WH

**CONTAINER ASSESSMENT — CORROSION STUDY  
OF HLW CONTAINER MATERIALS**

**QUARTERLY PROGRESS REPORT**

OCTOBER - DECEMBER 1981

**T.M. Ahn and P. Soo  
Principal Investigators**

**Contributors:**

B. S. Lee  
J. Woodward  
R. Sabatini

**Manuscript Completed — February 1982  
Date Published —**

**PREPARED BY THE NUCLEAR WASTE MANAGEMENT DIVISION  
DONALD G. SCHWEITZER, HEAD  
DEPARTMENT OF NUCLEAR ENERGY, BROOKHAVEN NATIONAL LABORATORY  
UPTON, NEW YORK 11973**

**PREPARED FOR THE UNITED STATES NUCLEAR REGULATORY COMMISSION  
OFFICE OF NUCLEAR REGULATORY RESEARCH  
UNDER CONTRACT NO. DE-AC02-76CH00016  
FIN NO. A-3237**

NUREG/CR-2317  
BNL-NUREG-51449  
Vol. 1, No. 4  
AN, WH

CONTAINER ASSESSMENT - CORROSION STUDY  
OF HLW CONTAINER MATERIALS

QUARTERLY PROGRESS REPORT  
OCTOBER - DECEMBER 1981

T. M. Ahn and P. Soo  
Principal Investigators

Contributors:

B. S. Lee  
J. Woodward  
R. Sabatini

Manuscript Completed - February 1982  
Date Published -

Prepared by the Nuclear Waste Management Division  
Donald G. Schweitzer, Head  
Department of Nuclear Energy, Brookhaven National Laboratory  
Upton, NY 11973

PREPARED FOR THE UNITED STATES NUCLEAR REGULATORY COMMISSION  
OFFICE OF NUCLEAR REGULATORY RESEARCH  
UNDER CONTRACT NO. DE-AC02-76CH00016  
FIN NO. A-3237

## ABSTRACT

Efforts in this quarter have been concentrated on the uniform and crevice corrosion, and hydrogen embrittlement of TiCode-12, which are considered to be potential corrosion failure modes in high level waste container systems.

The weight gain of TiCode-12 in WIPP Brine A is in good agreement with previous results from Sandia National Laboratory. The selective etching in weld heat-affected zones is considered to be responsible for the slower weight gain in the welded TiCode-12 and commercially pure (CP) titanium. The interaction of the oxide film with a salt compound precipitated from the solution makes it difficult to correlate the weight gain with the thickness of the oxide film.

The crevice corrosion of TiCode-12 in neutral brine solutions at 150°C has been identified by the observation of corrosion products and oxygen effects. The predominant oxide phase inside the crevice is  $TiO_2$ . In order to understand the mechanisms involved, crevice corrosion of CP titanium has also been studied. The interference colors observed seem to arise from a thickness variation of the corrosion products, which are composed of lower oxides as well as  $TiO_2$ . Variations of cathode/anode ratios and surface finishes affect the crevice corrosion rates. These observations suggest two possible hypotheses for the operating mechanism: variation of polarization inside the crevice and hydrolysis of dissolved metal ions.

The effect of the oxidizer (produced by radiolysis) on the open circuit corrosion potential has been studied for TiCode-12 in WIPP Brine B. For a concentration of 33,000 ppm  $HClO_3$ , change in the potential has been observed, which is an indication of enhanced susceptibility to stress corrosion cracking in this material.

Fractographic analysis of TiCode-12 and titanium in the study of internal hydrogen effects has been carried out using Scanning Electron Microscopy (SEM). Two types of cleavage occur as the strain rate is decreased or hydrogen level is increased. Interfacial failure features appear below the hydrogen level at which cleavage occurs. Present observations imply that the hydride is very likely to be responsible for the fracture process. Preliminary results show that gaseous hydrogen also affects the fracture mode in TiCode-12. Hydrogen analysis and hydrogen uptake tests are being initiated.

A limited amount of theoretical work has been performed on the construction of potential-pH diagrams for copper and lead at 100°C. Measurements have been made of the pressure build-up during gamma irradiation of brine and the gases generated were analyzed.

# CONTENTS

ABSTRACT. . . . .	iii
FIGURES . . . . .	vi
1. INTRODUCTION . . . . .	1
2. MATERIALS AND SOLUTIONS. . . . .	1
3. UNIFORM CORROSION. . . . .	1
4. CREVICE CORROSION. . . . .	2
4.1 TiCode-12 . . . . .	2
4.2 CP Titanium . . . . .	3
4.3 Probable Mechanism of Crevice Corrosion of CP Titanium and TiCode-12 . . . . .	3
5. WELD EFFECTS . . . . .	4
6. STRESS CORROSION CRACKING. . . . .	5
7. DETERMINATION OF POTENTIAL-pH DIAGRAM FOR Cu AND Pb IN AQUEOUS SOLUTION WITH HIGH CHLORIDE CONTENT AT HIGH TEMPERATURE. . . . .	6
8. HYDROGEN EMBRITTLEMENT . . . . .	6
8.1 Internal Hydrogen Effects . . . . .	6
8.2 Gaseous Hydrogen Effects. . . . .	9
8.3 Hydrogen Analysis . . . . .	9
8.4 Hydrogen Uptake . . . . .	9
9. RADIATION EFFECTS. . . . .	10
10. REFERENCES . . . . .	11

## FIGURES

1.	Weight Gain Data on CP Titanium and TiCode-12 in Brine A . . . . .	13
2.	Crevice Corrosion Product of TiCode-12 in Brine A at 200°C after Three Days' Exposure. . . . .	14
3.	Typical TEM Microstructure of Oxide Formed on TiCode-12. . . . .	15
4.	Oxide Scale Formed a. Inside and b. Outside of Crevice of TiCode-12 at 200°C in Brine A after Three Days' Exposure. . . . .	16
5.	Schematic Diagram of a Scale Formed in CP Titanium Crevice in Brine A at 150°C after 116 Days' Exposure . . . . .	17
6.	Schematic Diagram of a Scale Formed by Gas Flame Heating of CP Titanium . . . . .	18
7.	Titanium Oxide Formed in the Crevice of CP Titanium at 150°C in Brine A after 116 Days' Exposure . . . . .	18
8.	Crevice Samples with Various Cathode/Anode Ratios. . . . .	19
9.	Effect of Cathodic/Anode Ratio on the Corrosion Potential and Corrosion Current. . . . .	19
10.	Microstructure of Welded TiCode-12: a. Heat Affected Zone and b. The Unaffected Area . . . . .	20
11.	Recrystallized Alpha Phase Formed in Welded CP Titanium. . . . .	21
12.	a. Heat Affected Zone on a Typical Corroded Surface on Welded TiCode-12. . . . .	22
12.	b. The Unaffected Area on a Typical Corroded Surface on Welded TiCode-12. . . . .	23
13.	a. Heavily Heat Affected Zone on a Typical Corroded Surface on Welded CP Titanium. . . . .	24
13.	b. Lightly Heat Affected Zone on a Typical Corroded Surface on Welded CP Titanium. . . . .	25
14.	Schematic Diagram of the Relationship between Potential and Crack Tip Strain Rate, Determining Conditions Under which a Crack Tip Cracking Solution is Achieved and Maintained . . . . .	26
15.	Corrosion Potential Change of TiCode-12 by the Addition of an Oxidizer to Brine B at Room Temperature. . . . .	26

## FIGURES (Continued)

16.	a. Potential-pH Equilibrium Diagram for the System Copper-Brine A and B at 100°C. . . . .	27
16.	b. Potential-pH Equilibrium Diagram for the System Lead-Brine A and B at 100°C. . . . .	28
17.	a. Type I Cleavage and b. Type II Cleavage in Cathodically Charged and Subsequently Homogenized CP Titanium . . . . .	29
17.	c. Crack Arrest Marking in Cathodically Charged and Subsequently Homogenized CP Titanium . . . . .	30
18.	Beta Phase Observed in As Received TiCode-12 . . . . .	31
19.	Type I Cleavage of Cathodically Charged TiCode-12. . . . .	32
20.	a. Intergranular and b. Type II Cleavage in TiCode-12 Cathodically charged in Molten Salt. . . . .	33
20.	c. Serration at Boundary Between Alpha and Beta Phases in TiCode-12 Cathodically Charged in Molten Salt. . . . .	34
21.	Fractograph of Hydrogen Environment Assisted Cleavage of TiCode-12. . . . .	35
22.	Hydride Needles Formed at the Edges of Cathodically Charged CP Titanium. . . . .	36
23.	Pressure Build-Up During Gamma Irradiation of Brine A at a Dose Rate of Approximately $4 \times 10^6$ rads/hr and a Total Dose of $1.2 \times 10^9$ rads . . . . .	37

## 1. INTRODUCTION

Efforts in this quarter have been concentrated on the corrosion and hydrogen embrittlement of CP (commercially pure) titanium and TiCode-12. Particular emphasis was placed on the uniform and crevice corrosion, and hydrogen embrittlement of TiCode-12. These are considered to be potential corrosion failure modes. The identification of possible mechanisms are important since it forms the basis of analytical models for the long-term prediction of failure. Progress has also been made in the areas of stress corrosion cracking and radiation effects.

## 2. MATERIALS AND SOLUTIONS

The composition of CP titanium and TiCode-12 was reported in the last quarterly progress report.<sup>1</sup> Preparation techniques for Brine A were slightly modified by using borax ( $\text{Na}_2\text{B}_4\text{O}_7 \cdot 10\text{H}_2\text{O}$ ) instead of  $\text{HBO}_3$ . This eliminated a precipitation problem in the process of solution preparation. The pH of the new solution was 7.1 while that of the unmodified one was 6.5.

## 3. UNIFORM CORROSION

In the last quarterly progress report<sup>1</sup> some initial corrosion rates in Brine A were reported using weight change measurements. Subsequent SEM observation of the corroded surface revealed that a significant amount of precipitation from the solution had occurred. To reduce this artifact, all samples were cleaned in boiling water. Figure 1 shows a current compilation of weight gain data in Brine A. TiCode-12 is more resistant to uniform corrosion compared with CP titanium. In general, welded samples show less weight gain.\* This can be attributed to selective attack (see Section 5). The data on non-welded samples are in reasonable agreement with previous results.<sup>2</sup>

An attempt was made to measure the thicknesses of corrosion product films to confirm the assumption of titanium oxide formation during immersion. Generally, the observed thickness was greater (within a factor of 2) than predicted. EDAX was utilized to probe the scale. It showed the presence of significant amounts of Mg and Si incorporated in the film of both CP titanium and TiCode-12. These elements may exist in place of titanium or as complex compound(s) of Ti, Mg, and Si. In either case, it should be noted that: (1) simple weight changes cannot be converted to corrosion rates by assuming titanium oxide formation and (2) the passivation of titanium may not be maintained because of the existence of other elements within the oxide film. A comprehensive study of these films is currently under way.

---

\*One sample of electron-beam (EB) welded TiCode-12 showed a higher rate of weight gain than TiCode-12, which was reported in the last quarterly progress report.<sup>1</sup> This seems to be due to the precipitate effects mentioned above.

#### 4. CREVICE CORROSION

It was shown in the last quarterly progress report<sup>1</sup> that crevice corrosion of CP titanium had been confirmed and that there was an indication of crevice attack in TiCode-12 also. We have continued our study in order to understand the mechanisms giving rise to crevice corrosion of both CP titanium and TiCode-12 in brine solutions.

##### 4.1 TiCode-12

Initially, a crevice sample was immersed in Brine A and heated to 200°C. After three days, a distinct violet corrosion product was observable inside the crevice (Figure 2). By comparison, the outer surface showed no visible corrosion product. Subsequent testing at 150°C for 21 days also showed these features. This was the first observation, to our knowledge, of crevice corrosion of TiCode-12 in Brine A at 150°C.

The influence of oxygen content on crevice corrosion was subsequently studied by immersing the samples in both aerated and deaerated Brine A solutions at 150°C. After 21 days, the sample in the aerated solution showed the same types of corrosion product inside the crevice as before, while the deaerated solution gave rise to only a slight color change. This is consistent with results for crevice corrosion of CP titanium.<sup>3</sup> With an increase in temperature (170°C) the deaerated solutions gave a similar effect to the aerated solutions (i.e., both solutions gave significant crevice corrosion). In Brine A at both 150°C and 170°C, the central region of the crevice is violet and blue while the outer region is gold-yellow. In contrast, all the samples in Brine B showed gold-yellow colors only.

After the immersion, samples were dried in air and the surface films analyzed using EDAX in order to identify, if possible, any chemical changes taking place in the crevice. Samples in Brine A showed an indication of cation depletion inside the crevice when compared with the same analysis of the outside surface. However, further evidence is necessary because of the reaction of the cation with the titanium oxide (see Section 3).

The oxide film inside a crevice was stripped off chemically by etching (etchant: 5-parts HF, 10-parts HNO<sub>3</sub>, 30-parts lactic acid). The electron diffraction pattern of the film formed at 200°C showed mostly TiO<sub>2</sub> (Brookite or Anatase) with a trace of Ti<sub>3</sub>O<sub>5</sub>. A typical example of the microstructure of the oxide is shown in Figure 3. This result is quite different from that obtained with CP titanium which showed appreciable amounts of lower oxides (see Section 4.2). The modification of the oxides by the etchant is under consideration.

The thickness of the oxide film could also be observed with SEM after loosening the film by buckling the crevice and outside surfaces. The oxide film inside a crevice is slightly thicker than the film outside. The thickness inside the crevice is approximately 0.7 microns.

## 4.2 CP Titanium

The initial stage of crevice corrosion of CP titanium was studied in deaerated neutral Brine A solution at 150°C. Figure 5 shows the typical color bands of the scale inside the crevice. In order to determine the significance of the colors, a coupon of pure Ti (2 cm x 4 cm) was polished to 600 grit SiC paper and then heated in a gas flame. This produced many different colors on the surface of the coupon as shown in Figure 6. This coupon has the same sequence of colors as observed in crevice corroded specimens. These different colors could be caused either by the differing thickness of the oxide film<sup>4</sup> (interference colors) or by different types of oxides.<sup>5</sup> It is likely that they are interference colors caused by different thicknesses, based on the fact that the crystals in each colored region look similar in SEM photos with only grain size differences. In addition, there was no significant contrast obtained in the SEM. The crystal size observed in the greenish black region ranges up to 500 Å (Figure 7). Even when lower oxides are present or predominant, the interference colors can still be obtained by thickness variations.

The oxide films inside a crevice of several samples have been analyzed by Transmission Electron Microscopy (TEM). After statistical analysis of the diffraction pattern, there is a strong indication that lower oxides exist particularly in the form of Ti<sub>3</sub>O<sub>5</sub> with lesser possibilities of Ti<sub>2</sub>O<sub>3</sub> or TiO being present. These lower oxides seem to exist in outer parts of the crevice surface while strong TiO<sub>2</sub> peaks are observed in the central region.

Based on a macrocell formation hypothesis, the ratio of cathode area to anode area (C/A) could affect the anodic process inside the crevice. Three different crevice samples were prepared as shown in Figure 8, and were exposed at 150°C for 35 days in Brine A. The samples with higher C/A ratio (= 4) showed less corrosion compared with the lower C/A (= 1) ratio sample. Since the higher C/A ratio should give a higher corrosion rate<sup>6</sup> (Figure 9), the observation is contrary to that expected and may be a result of a shift in the corrosion potential inside the crevice above the active corrosion potential of pure titanium.

The effects of surface finishes were also studied. The outer surface of two CP titanium crevice samples (2 cm x 2 cm) were oxidized in air,<sup>7</sup> and heated at 150°C in Brine A solution for 26 days. Samples with oxidized surfaces showed less crevice corrosion (weak violet and brass colored film or almost no visible corrosion), while the regularly finished sample showed a more bluish film. The outside oxide scale may have reduced the cathodic reaction and caused less corrosion (Figure 9).

An attempt was made to measure the thickness of the corrosion product film by cracking the film. The film inside the crevice did not flake off easily and, consequently, it was not possible to measure its thickness.

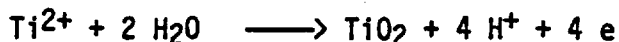
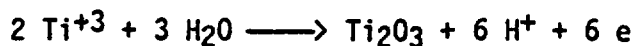
## 4.3 Probable Mechanism of Crevice Corrosion in CP Titanium and TiCode-12

Much of the theoretical interpretation of crevice corrosion has been associated with some sort of concentration cell,<sup>8</sup> which could be a metal-ion

cell, a differential aeration cell, an active-passive cell, and/or other concentrated cells such as hydrogen-ion, neutral salt, and inhibitor cells. The unified crevice corrosion mechanism postulated by Fontana and Greene<sup>6</sup> includes most of these phenomena and is described below.

Initially, the anodic dissolution (i.e.,  $M \longrightarrow M^+ + e^-$ ) and cathodic reduction (i.e.,  $O_2 + 2 H_2O + 4e^- \longrightarrow 4OH^-$ ) processes occur over the entire metal surface, including the crevice interior. The oxygen in the shielded crevice area is consumed after some incubation period. With the cessation of the cathodic hydroxide-producing reaction, however, the migration of mobile negative ions (i.e., chlorides) into the crevice area is required to maintain charge balance. The resulting metal chlorides hydrolyze to form insoluble metal hydroxides and free acid. Both the chloride anions and low pH accelerate crevice corrosion while the reduction reaction cathodically protects the exterior surfaces. Also, for active-passive metals that depend on protective oxide films for their corrosion resistance, the breakdown of passive and active corrosion in crevices are favored by an increased concentration of chloride and hydrogen ions. This model takes into account metal-ion concentration, oxygen depletion, hydrolysis and acidification, aggressive anion migration, and both active and active-passive dissolution behavior. A specific system requires some refinement in order to identify the predominant process.

An early study of TiCode-12 showed no crevice corrosion in Brines A and B.<sup>2</sup> Our observation of colored film formation, oxygen effects, and cation depletion support the existence of crevice corrosion of TiCode-12. At present, our results on CP titanium and TiCode-12 imply that the degree of polarization in the crevice region may be different depending on the position inside the crevice. An alternative interpretation is that the lower or higher oxides may have formed by hydrolysis of the metal ions:



Ti<sup>+3</sup> and Ti<sup>+2</sup> hydrolysis has been reported previously.<sup>9,10</sup> Further effort is needed in the identification of the specific mechanisms for the establishment of a mathematical description of crevice corrosion.

## 5. WELD EFFECTS

In near alpha titanium alloys, the temperature during welding is sufficient to reach the beta transus. Depending on the subsequent cooling rate, several different microstructures have been reported.<sup>11,12</sup> At very rapid rates of cooling, criss-cross networks of alpha martensite are formed while upon slow cooling, recrystallized, alpha platelets are formed<sup>11</sup> often with eutectoid phases (alpha + Ti<sub>2</sub>Ni).<sup>12</sup> The structure of electron beam welded CP titanium and TiCode-12 have been considered and their response to uniform and crevice corrosion have been studied by optical microscopy.

Two 0.5 x 2.2-cm coupons were electron beam welded together in a vacuum to form a coupon 1 x 2 cm in size.\* TiCode-12 showed a significant amount of martensite or recrystallized alpha platelet formation in the fused zone (Figure 10a). Away from the heat affected zone (HAZ) the microstructure remained unchanged (Figure 10b). On the other hand, the CP titanium coupon was heat affected over the whole sample showing recrystallized alpha platelets (Figure 11), possibly with a minor eutectoid phase.

In TiCode-12, there appeared to be a selective etching of the recrystallized structure (Figure 12a) compared to fairly uniform etching away from the HAZ (Figure 12b). The creviced sample did not show any distinct difference between the inside and outside of the crevice. Similar features were also observed in CP titanium (Figure 13). Preferential attack seems to occur along the boundaries between the beta and recrystallized alpha platelet in CP titanium.

The results give general information on the microstructure of welded CP titanium and TiCode-12 and the preferential attack of the newly formed phases produced by welding. Longer time exposures are currently being conducted to find out whether continuous attack will be prevented by the onset of repassivation. If not, this may be another type of localized corrosion which needs to be considered in connection with long-term containment of nuclear waste.

## 6. STRESS CORROSION CRACKING

In this quarter, our efforts have been on the potential effect of radiolytically generated oxidizer(s) on the stress corrosion cracking (SCC) of TiCode-12 in brine solutions.

The anodic dissolution mechanism of stress corrosion cracking can be represented as a crack tip strain rate and repassivation rate effect. Some balance between the two rates is an essential feature of the crack propagation rate.<sup>13-15</sup> One of the effects of an oxidizer on SCC is to change the repassivation rate via a corrosion potential shift. Scully<sup>13,15</sup> has developed a relationship between the potential (E) and crack tip strain rate, determining conditions under which a crack tip cracking solution is achieved and maintained as shown in Figure 14. There is a range of potentials and strain rates over which SCC occurs.

An earlier study at Sandia<sup>2</sup> showed some fractographic evidence for SCC of TiCode-12 in brines though the mechanical properties did not change significantly. This suggests the possibility that the testing condition used may have been at the limit of SCC susceptibility.

---

\*For metallographic observations, samples were mounted and etched after polishing.

Among the oxidizers produced by radiolysis in brine, such as  $H_2O_2$ ,  $ClO_3^-$ ,  $ClO_4^-$ , the strongest oxidizer ( $ClO_3^-$ ) was chosen as an additive to Brine B to determine the influence of such species on the open circuit corrosion potential at room temperature. At a 33,000 ppm  $ClO_3^-$  concentration, a corrosion potential change was observed as shown in Figure 15. The concentration of  $ClO_3^-$  used was about 8% of the expected concentration of  $ClO_3^-$  when all  $Cl^-$  dissolved in Brine B is converted to  $ClO_3^-$  by radiolysis. This indicates that the rise of corrosion potential might be much more significant under real repository conditions leading to an increase in the susceptibility of TiCode-12 to SCC in Brine B.

The implication of this result is that radiation may enhance the SCC susceptibility entirely by directing only the anodic dissolution process. Besides the anodic dissolution process, hydrogen induced SCC also will be enhanced by radiolysis since hydrogen is also generated and can then lead to delayed failure.<sup>1</sup>

#### 7. DETERMINATION OF POTENTIAL-pH DIAGRAM FOR Cu AND Pb IN AQUEOUS SOLUTION WITH HIGH CHLORIDE CONTENT AT HIGH TEMPERATURE

A small continuing effort has been given to generate a potential-pH diagram for Cu and Pb in aqueous solution with high chloride content at 100°C. New domains of  $Cu(OH)_2$ ,  $CuCl$  and  $Cu_2O$  are still observed with  $CuO$  and  $Cu_2O$  domains shifted to higher pH regions compared to the diagram at room temperature (Figure 16a). If the potential is negative (vs hydrogen voltage  $V_H$ ), dissolution of copper to form aqueous copper chloro-complexes appear to be highly probable. In the case of lead (Figure 16b) the stabilities of  $PbSO_4$  and  $PbCl_2$  are observed at 100°C as in the case at room temperature.

#### 8. HYDROGEN EMBRITTLEMENT

##### 8.1 Internal Hydrogen Effects

In the last quarterly progress report slow strain rate embrittlement and impact embrittlement were reported in cathodically hydrogen charged CP titanium and TiCode-12 in tension and buckling tests.<sup>1</sup> Continuing efforts have been made to characterize the fracture modes of these samples by analyzing the fractographs. Such an approach is necessary in order to identify the mechanism(s) involved in the hydrogen induced cracking of TiCode-12. An analytical description of this cracking process is achievable provided the mechanism responsible can be identified from the following possibilities:

1. stress assisted hydride formation at the crack tip and subsequent crack propagation along the matrix hydride interface;<sup>16</sup>
2. titanium hydride enhanced creep;<sup>19</sup>
3. preferential segregation of hydrogen in the beta phase and hydride precipitation at the alpha/beta interface leading to alpha/beta interfacial separation;<sup>18</sup>

4. slip inhibition by interstitial hydrogen;<sup>19</sup>
5. decohesion model;<sup>21</sup>
6. hydrogen gas embrittlement.<sup>21</sup>

Tables 1 and 2 are summaries of the fractographic observations.

Table 1  
Fractographic Analysis of CP Titanium\*†

Strain Rate	As Received		Cathodically Charged and Subsequently Homogenized	
	Description	Figure	Description	Figure
1.2x10 <sup>-2</sup> /sec	Ductile dimples	--	Ductile dimples, type II cleavage	--
2.5x10 <sup>-5</sup> /sec	Mostly ductile dimples, becoming intergranular	--	Ductile dimples, type I cleavage	17a (type I)
			and type II cleavage,	17b (type II)
			crack arrest	17c

\*"Cathodically charged": in 10% sulfuric acid with 3.1x10<sup>-3</sup> M Na<sub>4</sub>P<sub>2</sub>O<sub>7</sub>.  
†Hydrogen levels are in the following order: as received < cathodically charged and subsequently homogenized < cathodically charged < cathodically charged (molten salt).

Table 2  
Fractographic Analysis of TiCode-12

Strain Rate	As Received		Cathodically Charged and Subsequently Homogenized		Cathodically Charged		Cathodically Charged (Molten Salt)	
	Description	Figure	Description	Figure	Description	Figure	Description	Figure
1.2x10 <sup>-2</sup> /sec	Ductile dimples	--	Ductile dimples	--	Ductile dimples	--	(Buckling) interfacial failure, type II cleavage, serrated interface	20a 20b 20c
2.5x10 <sup>-5</sup> /sec	Ductile dimples, beta phase	18	Ductile dimples, becoming interfacial failure type I cleavage					
2.4x10 <sup>-5</sup> /sec					Ductile dimples, becoming interfacial failure, type I and II cleavage	19		

Ductile dimples are predominant in high strain rate tests. Two types of cleavage occur (Figures 17a, 17b, 19, and 20b) as the strain rate is decreased or hydrogen level is increased. Tentatively, these will be called type I and type II cleavages. Both types of cleavage are distributed very inhomogeneously and are more frequently observed as the hydrogen level increases. Type II cleavage tends to appear at higher hydrogen levels than type I cleavage. Intergranular features (Figures 20a) appear below the hydrogen level at which cleavage occurs. On the other hand, the observed beta phase<sup>18</sup> and ductile dimples implies the alpha phase fractures at low hydrogen level. Serrated interfaces are frequently observed (Figure 20c) implying interfacial separation. Crack arrest markings are observed suggesting intermittent crack propagation (Figure 17c).

Since no significant difference is observed between CP titanium and TiCode-12, hydride formation seems to be responsible for the fracture. This implies that slip inhibition, decohesion or gas embrittlement is unlikely though confirmation is needed by the measurement of a yield drop or incubation time for fracture.<sup>22</sup> On this hypothesis, alpha phase cleavage at low hydrogen levels and alpha-beta interfacial cracking at higher hydrogen levels may be operative.<sup>16,22,23,24-26</sup> The absence of distinct serpentine features<sup>27</sup> may discount a creep mechanism also. Currently, more well defined fracture mechanics samples are being tested for confirmation of the present general observations.

## 8.2 Gaseous Hydrogen Effects

A preliminary study on the behavior of as received single-edged-notched TiCode-12 strained at rates between  $10^{-8}$  and  $10^{-4}s^{-1}$  in low pressure ( $\sqrt{2}$  atmospheres) of hydrogen gas at room temperature indicates that a hydrogen environment promotes cleavage type failure (Figure 21). The influence of gaseous hydrogen on the maximum load is probably small, a result which has been observed for other near alpha Ti alloys tested in the as received condition.<sup>24</sup> The study is being extended to determine the role of temperature. Results to date suggest that the effect of hydrogen on the failure mode is increased with increasing temperature. The mechanism(s) by which gaseous hydrogen affects the behavior of TiCode-12 at slow strain rates and under creep conditions will be examined.

## 8.3 Hydrogen Analysis

Hot vacuum extraction and mass spectrometric analysis were used to determine the hydrogen level of as received CP titanium and TiCode-12. Three to four samples were used to check the reproducibility as shown in Table 3. The analytical method will be expanded to find the maximum extent to which hydrogen can be absorbed. Hydride formation (Figure 22) makes it difficult to estimate the maximum amount of hydrogen in solution.

## 8.4 Hydrogen Uptake

It is generally known that hydrogen is absorbed in metals in the atomic form.<sup>28</sup> The presence of TiO<sub>2</sub> surface films reduces the degree of hydrogen

Table 3

Hydrogen Levels in As Received Titanium and TiCode-12 Samples

TiCode-12 (ppm)	32	36	33	35
CP titanium (ppm)	92	72	75	--

penetration.<sup>29</sup> The existence of crevice corrosion may produce sufficient active anodic areas enabling the dissociation of hydrogen molecules to take place, this dissociation being a necessary precursor for hydrogen uptake of crevice samples in brine solutions. At present, samples are being tested at 150°C in Brine B in the presence of hydrogen at a pressure of 220 psi.

#### 9. RADIATION EFFECTS

In Figure 23 are shown initial results on pressure increases in capsules containing Brine A and air exposed to gamma irradiation. The dose rate is  $\sim 4 \times 10^6$  rads/hr and the total dose is  $1.2 \times 10^9$  rads. Table 4 shows gas analysis results using mass spectrometry. The potential problem of inhomogeneous gas distribution is under study.

Table 4

Composition of Gas in Capsule Containing Brine B and Air after Gamma Irradiation to a Dose of  $1.2 \times 10^9$  Rads

	O <sub>2</sub>	N <sub>2</sub>	H <sub>2</sub>	CO <sub>2</sub>	H <sub>2</sub> O	Ar
Vol. %	42.8	39.1	15.4	1.98	0.57	0.16

## 10. REFERENCES

1. T. M. Ahn, P. Soo, B. S. Lee, J. Woodward, R. C. Newman, and S. Aronson "Container Assessment - Corrosion Study of HLW Container Materials, Quarterly Progress Report, July-September 1981," BNL Report, BNL-MUREG-51449, Vol. 1, No. 3, (1981).
2. J. W. Braithwaite, N. J. Magnani, and J. W. Munford "Titanium Alloy Corrosion in Nuclear Waste Environments," Sandia Report, SAND 79-2023C (1979).
3. J. C. Griess, Jr. "Crevice Corrosion of Titanium in Aqueous Salt Solutions," Corrosion-NACE 24, 96 (1968).
4. U. R. Evans, in The Corrosion and Oxidation of Metals: Scientific Principles and Practical Applications, Edward Arnold Ltd., 1960.
5. K. Hauffe in Oxidation of Metals, Plenum Press, New York, NY, 1965.
6. M. G. Fontana and N. D. Greene, Corrosion Engineering, Second Edition, McGraw-Hill, New York, 1978.
7. R. W. Schutz and L. C. Covington "Effect of Oxide Films on the Corrosion Resistance of Titanium," Corrosion 37, 585 (1981).
8. W. D. France, Jr. "Crevice Corrosion of Metals", in Localized Corrosion-Cause of Metal Failure, ASTM, STP 516 (1972).
9. E. J. Kelly "Anodic Dissolution and Passivation of Titanium in Acidic Metal III Chloride Solutions", J. Electrochem. Soc. 126, 2064 (1979).
10. L. L. Shreir "Localized Corrosion," in Corrosion Vol. 1, L. L. Shreir, Ed., (Newnes-Butterworth, 1979).
11. J. Gordine "Weld Heat-Affected Zones in Titanium-6Al-2Cb-1Ta-1Mo," Welding Research Supplement, 117-S (1974).
12. J. A. S. Green and P. S. Kotral "Influence of Microstructure on the Corrosion Behavior of Ti-2% Ni on Hot Acidic Chloride Solutions, with Particular Reference to Weld Regions," Corrosion-NACE, 420 (1972).
13. J. C. Scully "Environmental Variables and Corrosion Crack Propagation Rates," in Environmental Degradation of Engineering Materials in Aggressive Environments, M. R. Louthan, Jr., R. P. McNitt, and R. D. Sission, Jr., Eds., (VPI, VA, 1981).
14. J. C. Scully "Stress Corrosion Crack Propagation: A Constant Change Criterion," Corrosion Science 15, 207 (1975).
15. J. C. Scully "The Interaction of Strain-Rate and Repassivation Rate in Stress Corrosion Crack Propagation," Corrosion Science 20, 997 (1980).

16. N. R. Moody and W. W. Gerberich "Hydrogen-Induced Slow Crack Growth in Ti-6Al-6V-2Sn," Met. Trans. A. 11A, 973 (1980).
17. D. N. Williams "Subcritical Crack Growth Under Sustained Load," Met. Trans. A. 5, 2351 (1974).
18. D. A. Meyn, paper presented at TMS-AIME Fall Meeting in Niagra Falls, NY, September 1976.
19. H. G. Vaughan and M. E. deMorton, Brit Welding I 36, 40 (1957).
20. A. R. Troiano, Trans. ASM 52, 54 (1960).
21. T. B. Cox and J. P. Gudas "Investigation of the Fracture of Near-Alpha Titanium Alloys in High Pressure Hydrogen Environments," in Effect of Hydrogen on Behavior of Materials, Eds., A. W. Thompson and I. M. Bernstein, (AIME, New York, 1975).
22. D. A. Meyn "Effect of Hydrogen on fracture and Inert-Environment Sustained Load Cracking Resistance of  $\alpha$ - $\beta$  Titanium Alloys," Met. Trans. 5, 319 (1973).
23. D. A. Meyn "Effect of Hydrogen Content on Inert Environment Sustained Load Crack Propagation Mechanisms of Ti-6Al-4V," ibid. ref. 13.
24. H. G. Nelson, D. P. Williams, and J. E. Stein "Environmental Hydrogen Embrittlement of a  $\alpha$ - $\beta$  Titanium Alloy Effect of Microstructure," Met. Trans. 3, 275 (1972).
25. G. H. Koch, A. J. Bursle, R. Liu, and E. N. Pugh "A Comparison of Gaseous Hydrogen Embrittlement, Slow Strain Rate Hydrogen Embrittlement, and Stress Corrosion Cracking in Ti-8Al-1Mo-1V," Met. Trans. 12A, 1833 (1981).
26. S. M. L. Sastry, R. J. Lederich, and B. B. Rath "Subcritical Crack Growth Under Sustained Load in Ti-6Al-6V-2Sn," Met. Trans. 12A, 83 (1981).
27. R. R. Boyer and W. F. Spurr "Characteristics of Sustained-Load Cracking and Hydrogen Effect in Ti-6Al-4V," Met. Trans. A. 9A, 23 (1978).
28. L. C. Covington and N. G. Feige "A Study of Factors Affecting the Hydrogen Uptake Efficiency of Titanium in Na(OH) Solutions," in Localized Corrosion-Cause of Metal Failure, ASTM, STP 516 (1972).
29. B. Kasemo and E. Tornquist "The Kinetics of Hydrogen Interaction with  $TiH_x$  Films,  $0 \leq x \leq 2$ ," Applications of Surface Science 3, 307 (1979).

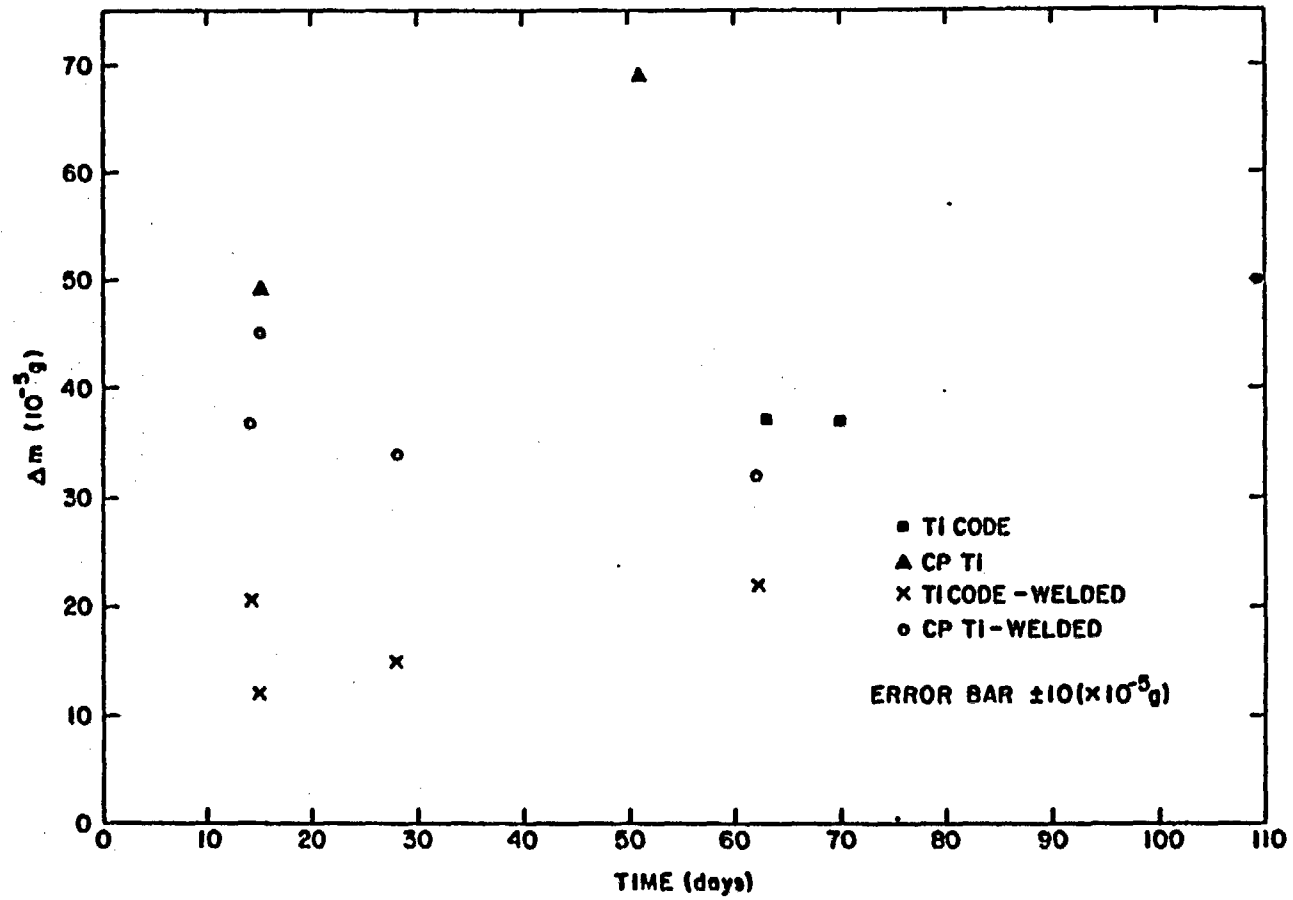
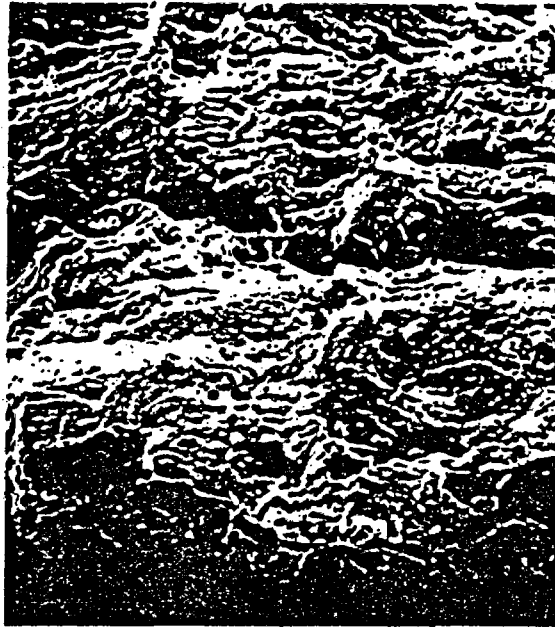
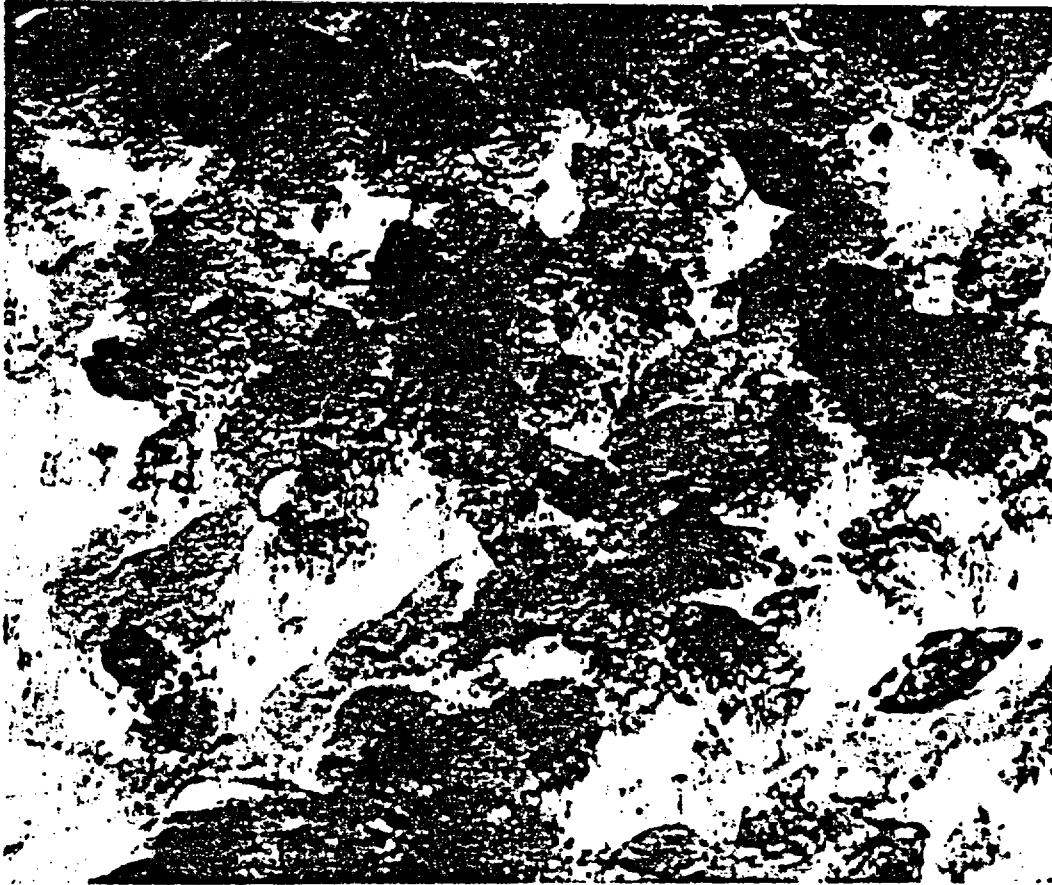


Figure 1. Weight gain data on CP titanium and TiCode-12 in Brine A.



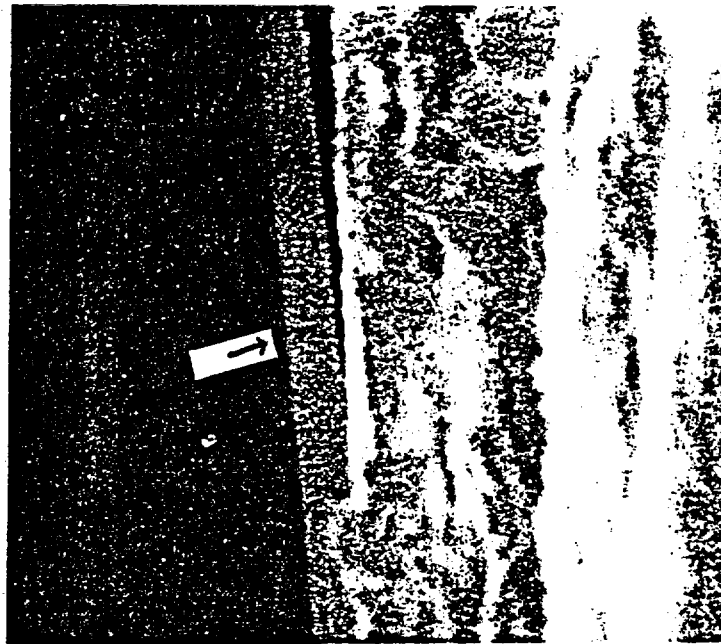
—  
10  $\mu$

Figure 2. Crevice corrosion product of TiCode-12 in Brine A at 200°C after three days' exposure.



0.1 μ

Figure 3. Typical TEM microstructure of oxide formed on TiCode-12.



1  $\mu$

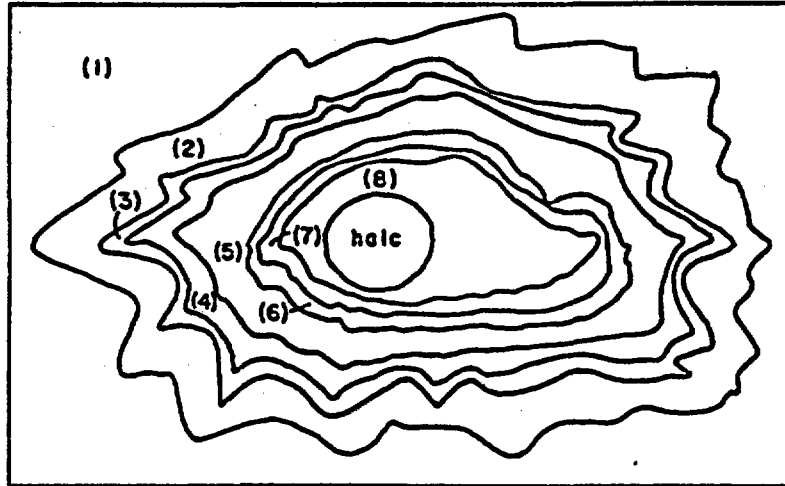
a.



1  $\mu$

b.

Figure 4. Oxide scale formed a. inside and b. outside of crevice of TiCode-12 at 209°C in Brine A after three days' exposure.



- |                         |                     |
|-------------------------|---------------------|
| 1. shiny (metallic)     | 5. shiny (metallic) |
| 2. brass yellow (light) | 6. brass yellow     |
| 3. violet               | 7. violet           |
| 4. blue                 | 8. greenish black   |

Figure 5. Schematic diagram of a scale formed in CP titanium crevice in Brine A at 150°C after 116 days' exposure.

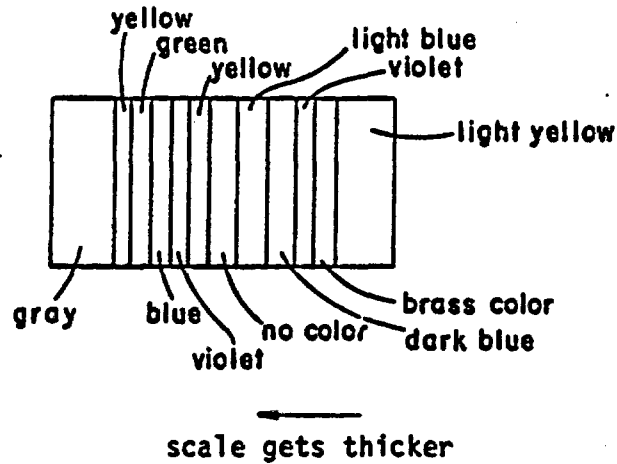


Figure 6. Schematic diagram of a scale formed by gas flame heating of CP titanium.

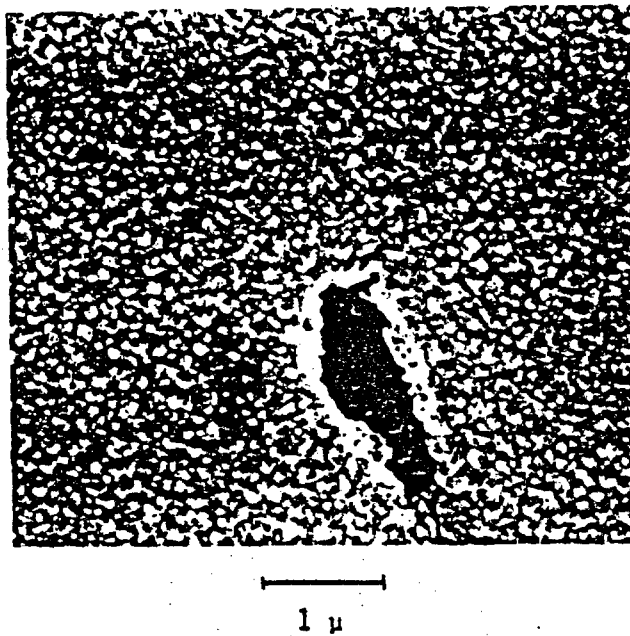


Figure 7. Titanium oxide formed in the crevice of CP titanium at 150°C in Brine A after 116 days' exposure.

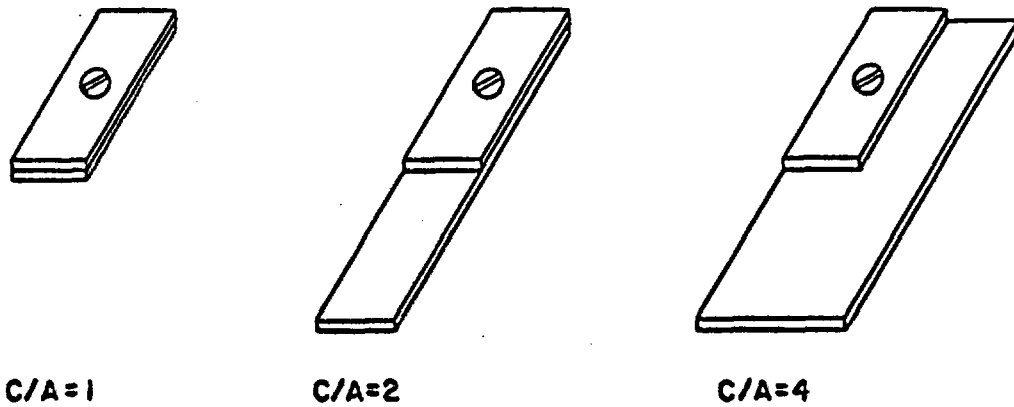


Figure 8. Crevice samples with various cathode/anode ratios.

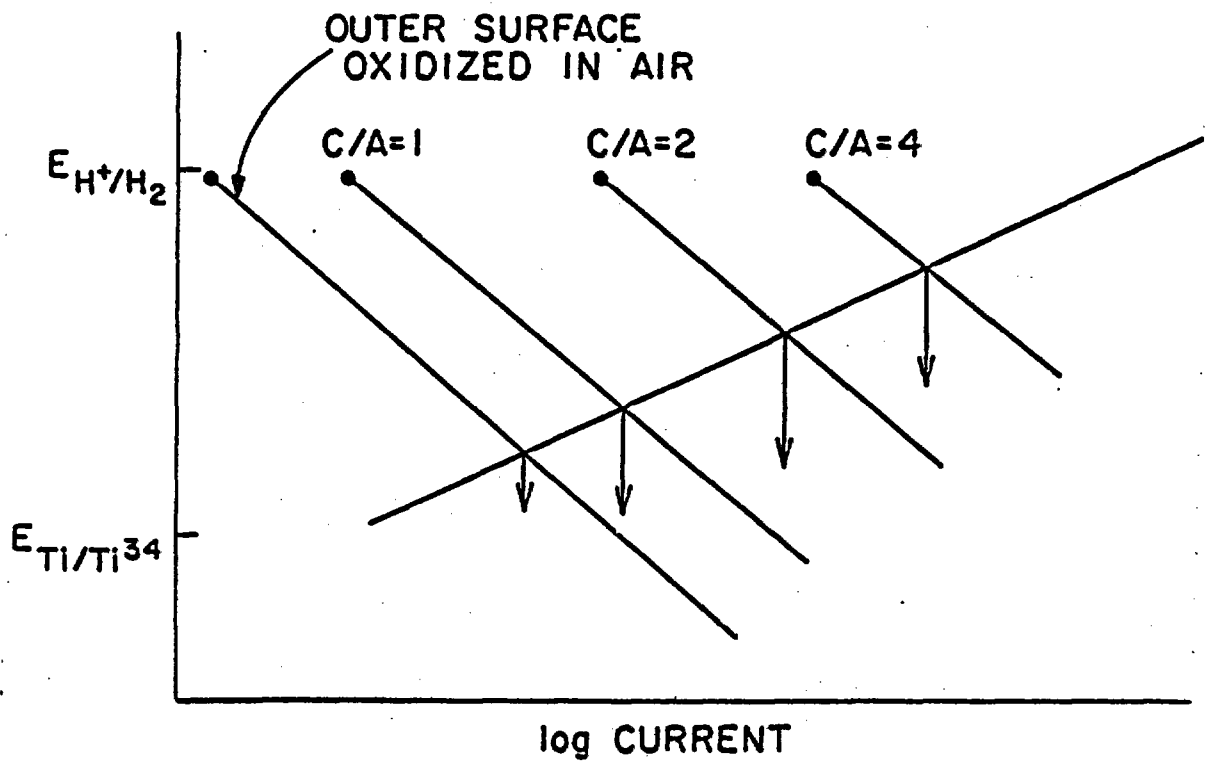
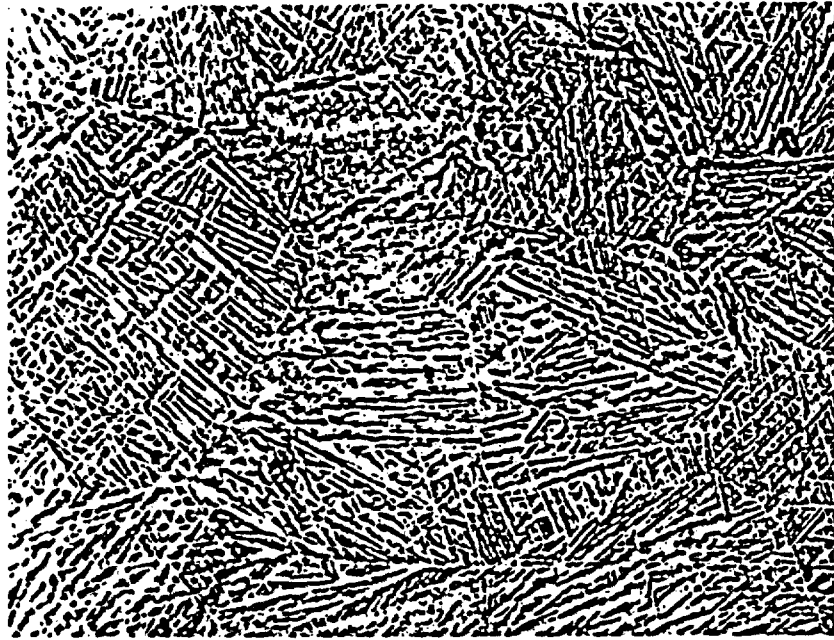
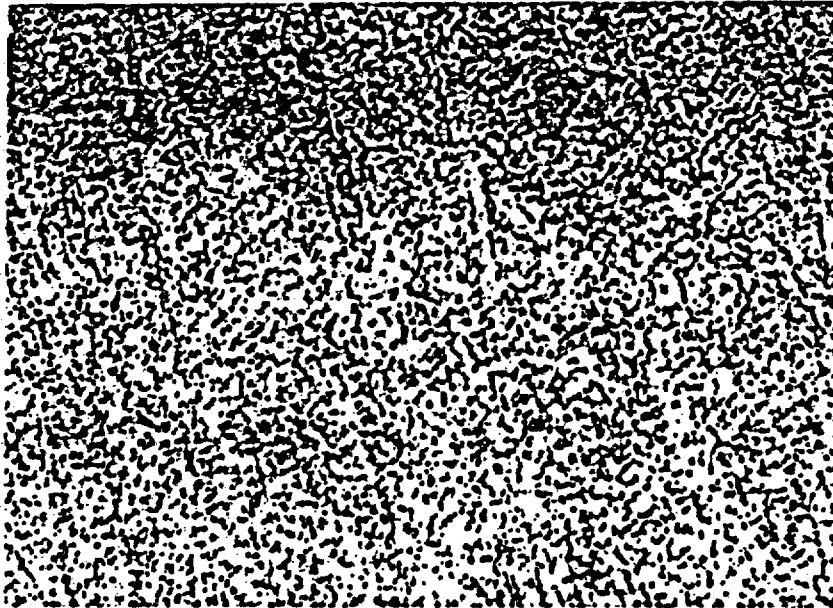


Figure 9. Effect of cathodic/anode ratio on the corrosion potential and corrosion current. Anodic curve is for titanium dissolution while cathodic curves are for hydrogen evolution reactions at various C/A ratios. The arrows indicate the corrosion currents.



50  $\mu$

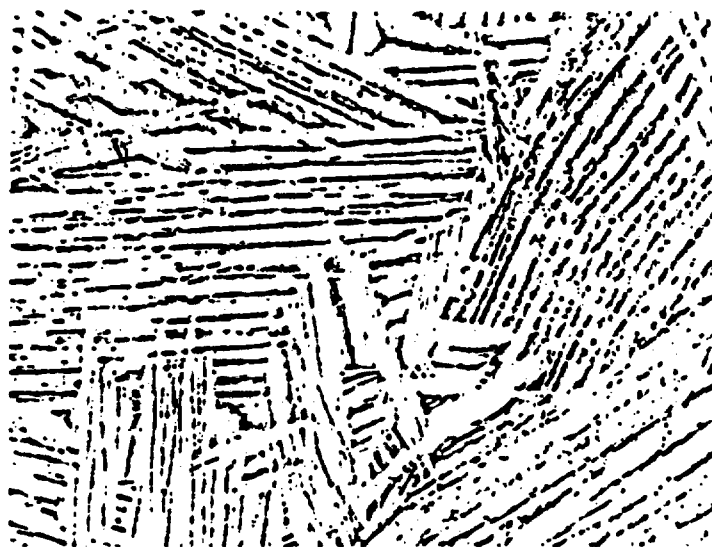
a.



50  $\mu$

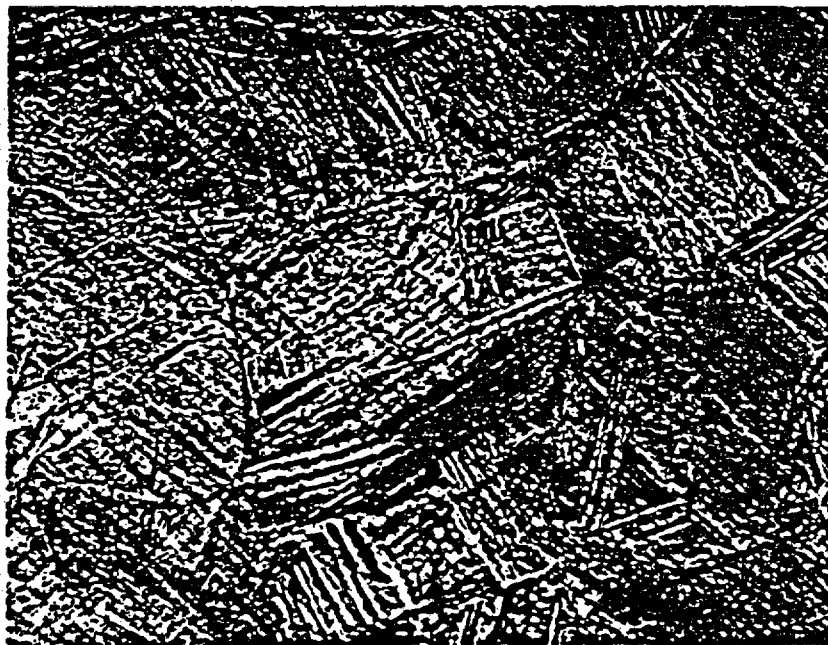
b.

Figure 10. Microstructure of welded TiCode-12: a. heat affected zone and b. the unaffected area.



50  $\mu$

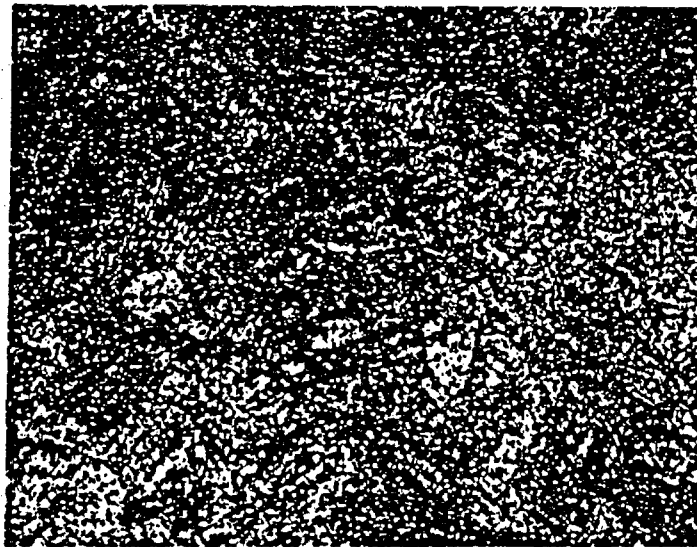
Figure 11. Recrystallized alpha phase formed in welded CP titanium.



100  $\mu$

a.

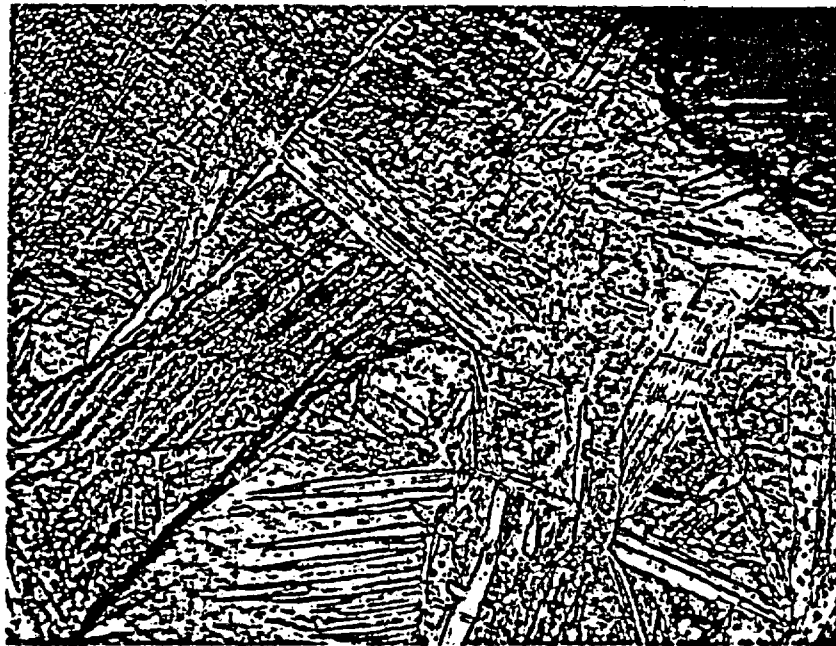
Figure 12. Heat affected zone on a typical corroded surface on welded TiCode-12.



100 μ

b.

Figure 12. The unaffected area on a typical corroded surface on welded TiCode-12.



100  $\mu$

a.

Figure 13. Heavily heat affected zone on a typical corroded surface on welded CP titanium.



10  $\mu$

b.

Figure 13. Lightly heat affected zone on a typical corroded surface on welded CP titanium.

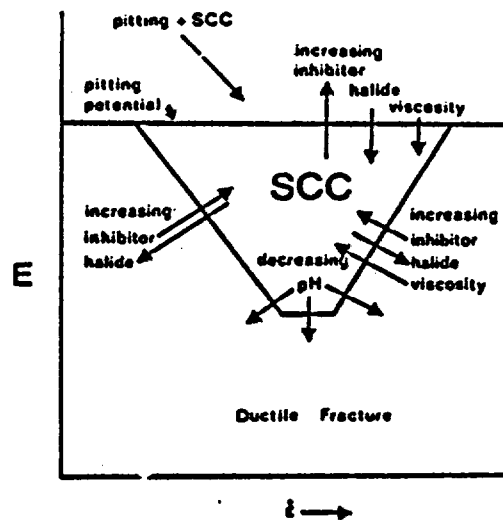


Figure 14. Schematic diagram of the relationship between potential and crack tip strain rate, determining conditions under which a crack tip cracking solution is achieved and maintained.<sup>13</sup>

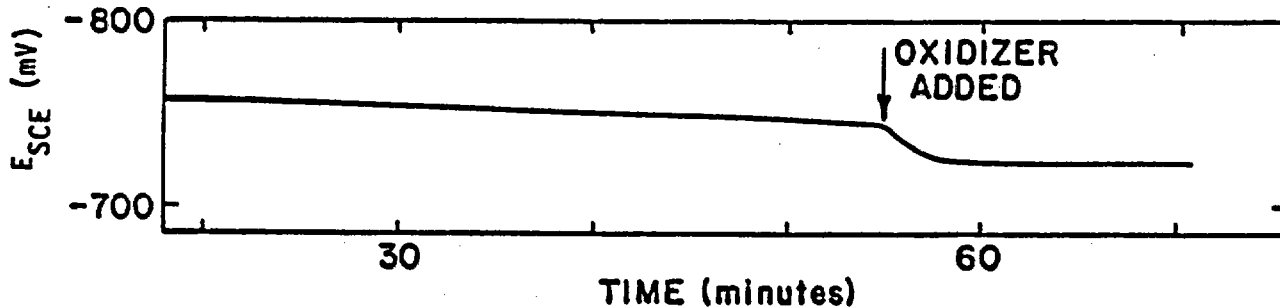
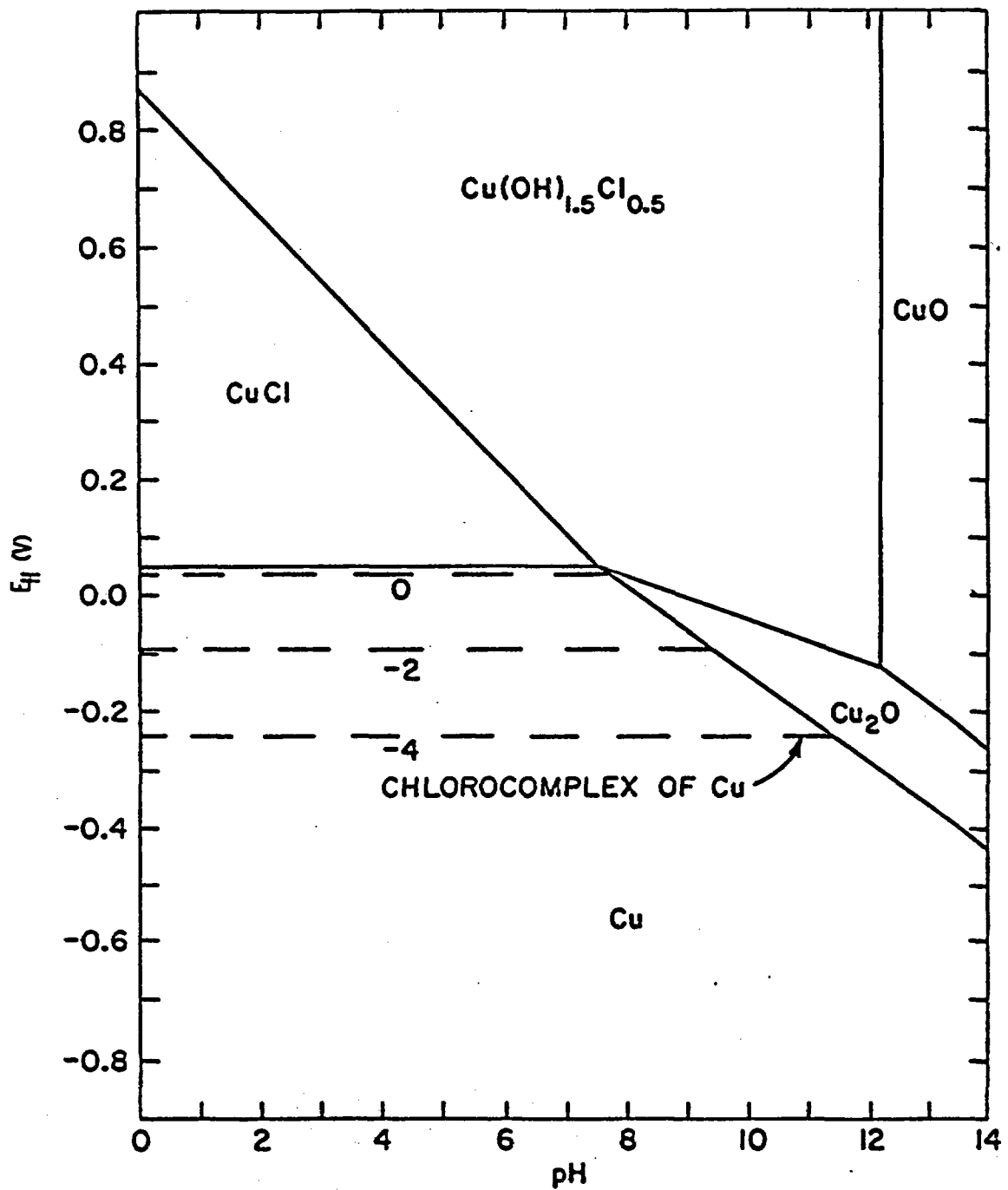
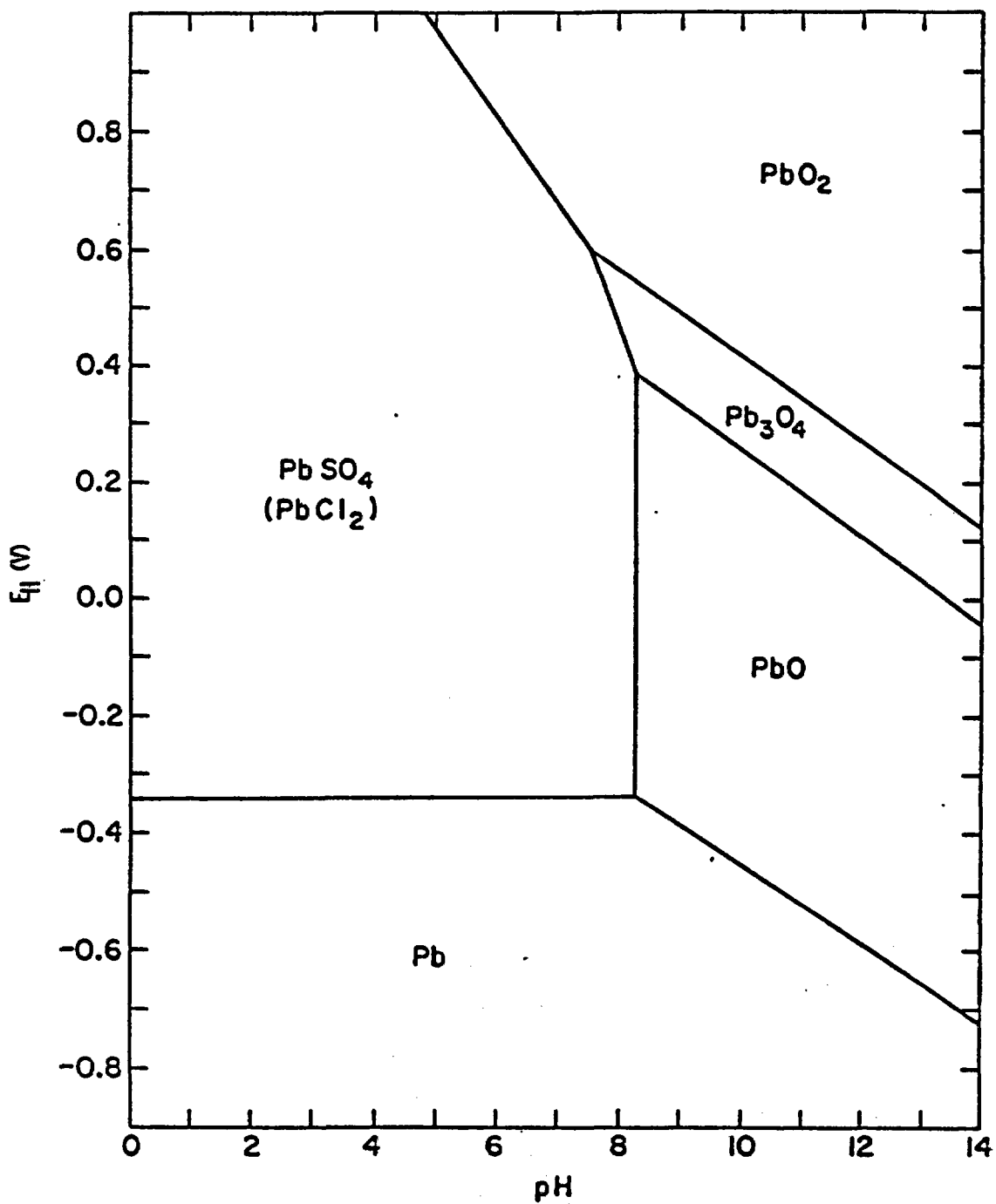


Figure 15. Corrosion potential change of TiCode-12 by the addition of an oxidizer to Brine B at room temperature.



a.

Figure 16. Potential-pH equilibrium diagram for the system copper-Brine A and B at 100°C.



b.

Figure 16. Potential-pH equilibrium diagram for the system lead-Brine A and B at 100°C.



—  
1.0  $\mu$   
a.



—  
1.0  $\mu$   
b.

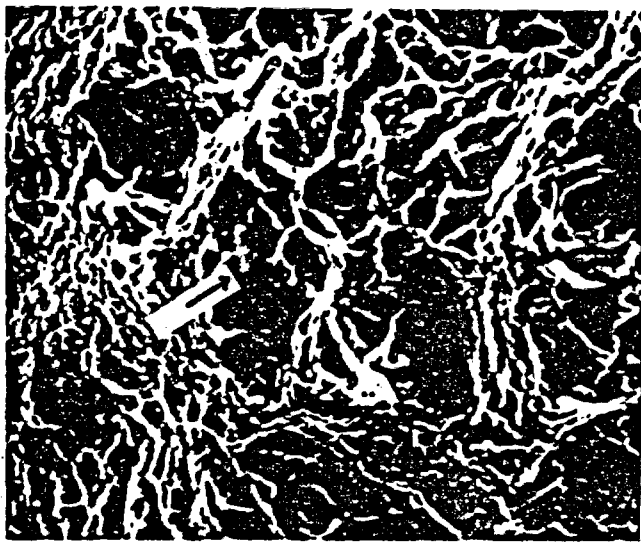
Figure 17. a. Type I cleavage and b. type II cleavage in cathodically charged and subsequently homogenized CP titanium.



10  $\mu$

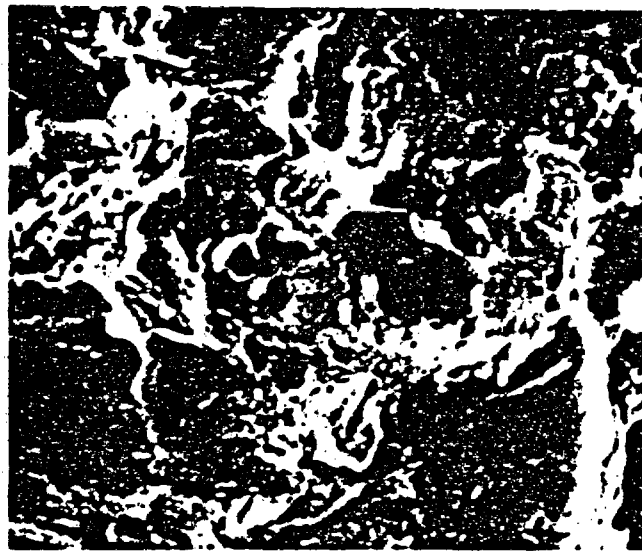
c.

Figure 17. Crack arrest marking in cathodically charged and subsequently homogenized CP titanium.



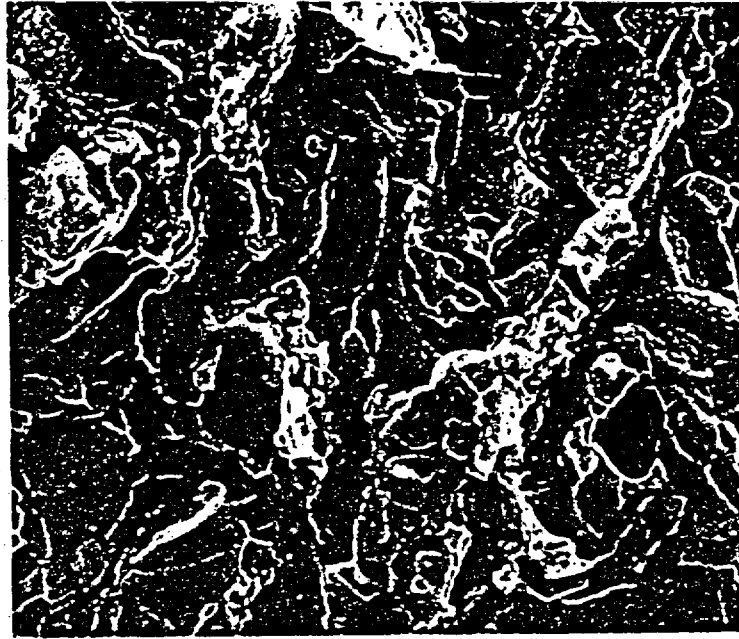
10  $\mu$

Figure 18. Beta phase observed in as received TiCode-12.



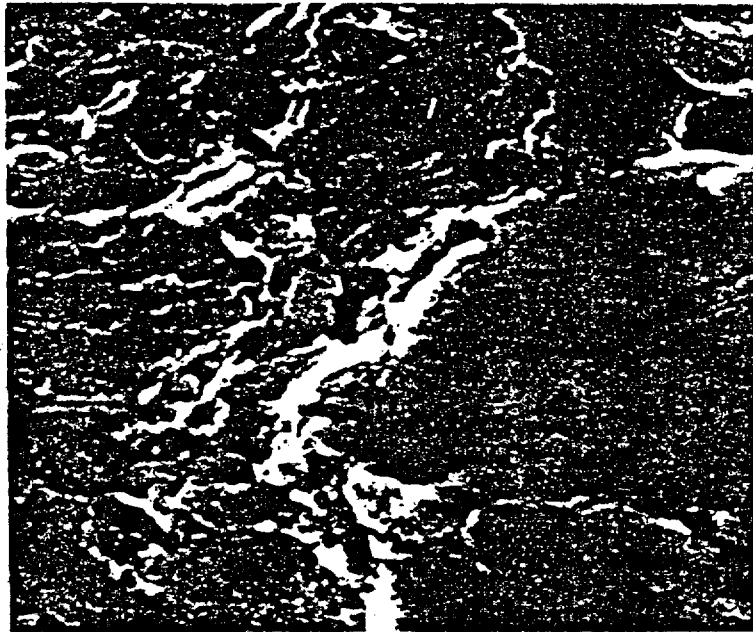
—  
1.0  $\mu$

Figure 19. Type I cleavage of cathodically charged TiCode-12.



10  $\mu$

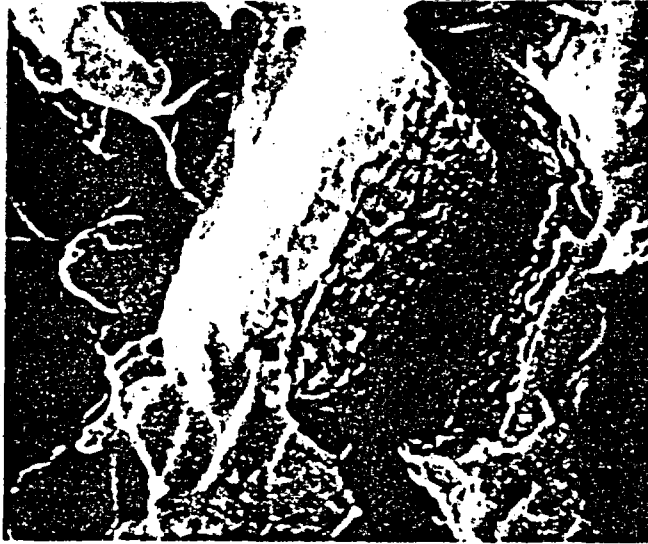
a.



1  $\mu$

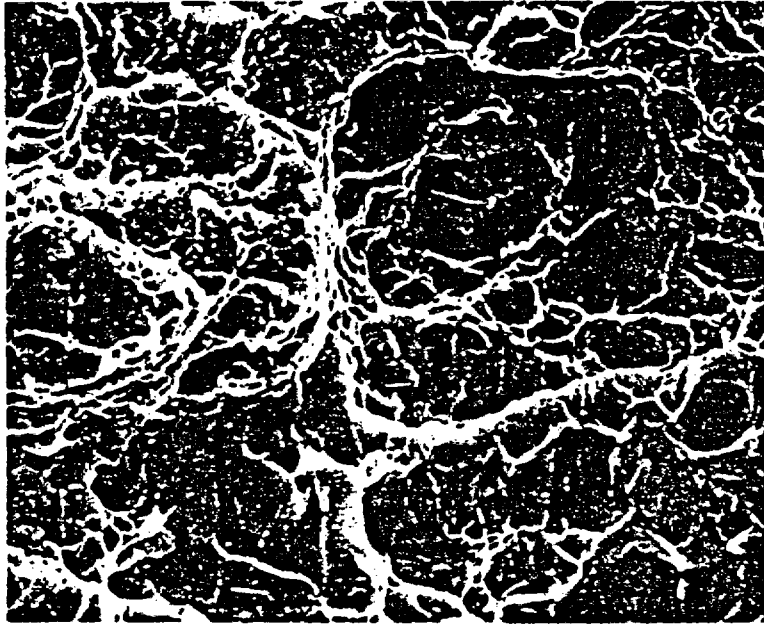
b.

Figure 20. a. Intergranular and b. type II cleavage in TiCode-12 cathodically charged in molten salt.

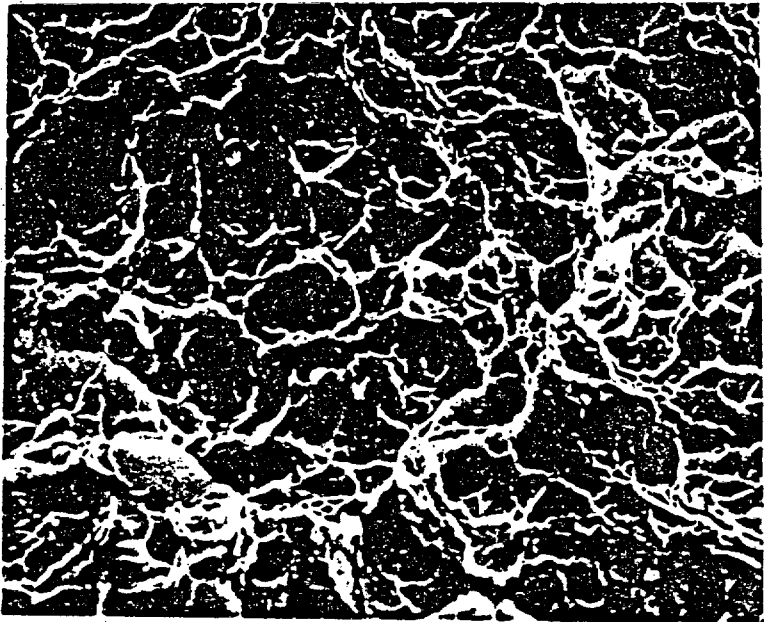


┌─┐  
1.0  $\mu$   
c.

Figure 20. Serrations at boundary between alpha and beta phases in TiCode-12 cathodically charged in molten salt.



10 μ



10 μ

Figure 21. Fractograph of hydrogen environment assisted cleavage of TiCode-12.



100 μ

Figure 22. Hydride needles formed at the edges of cathodically charged CP titanium.

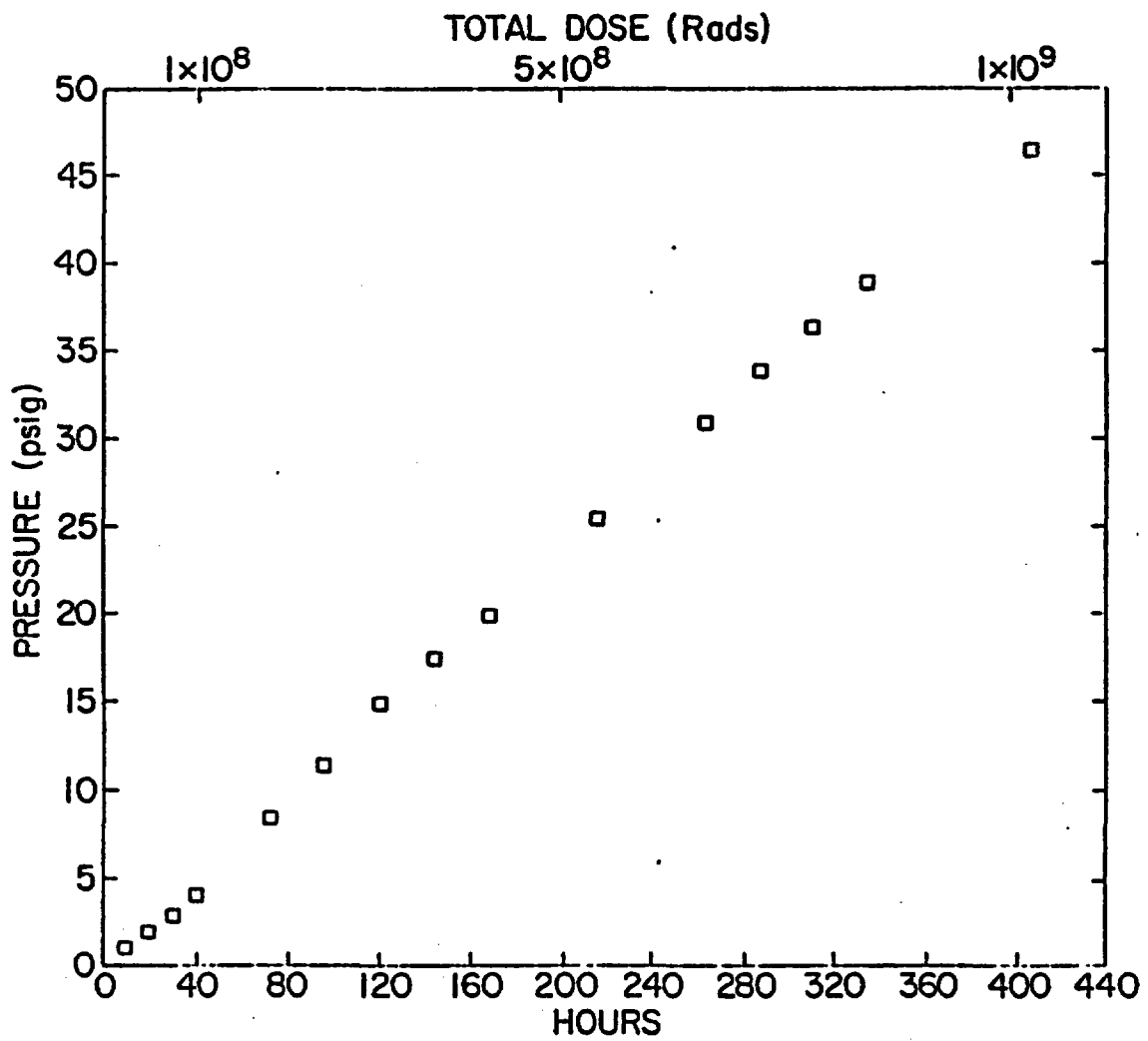


Figure 23. Pressure build-up during gamma irradiation of Brine A at a dose rate of approximately  $4 \times 10^6$  rads/hr and a total dose of  $1.2 \times 10^9$  rads.

NUREG/CR-2317  
BNL-NUREG-51449  
Vol. 2, No. 1  
AN, WE

CONTAINER ASSESSMENT - CORROSION STUDY  
OF HLW CONTAINER MATERIALS

QUARTERLY PROGRESS REPORT  
JANUARY-MARCH 1982

T. M. Ahn and P. Soo  
Principal Investigators

Contributors:

B. S. Lee  
J. Woodward  
R. Sabatini

Manuscript Completed - April 1982  
Date Published -

Prepared by the Nuclear Waste Management Division  
Donald G. Schweitzer, Head  
Department of Nuclear Energy, Brookhaven National Laboratory  
Upton, NY 11973

PREPARED FOR THE UNITED STATES NUCLEAR REGULATORY COMMISSION  
OFFICE OF NUCLEAR REGULATORY RESEARCH  
UNDER CONTRACT NO. DE-AC02-76CH00016  
FIN NO. A-3237

## ABSTRACT

Crevice corrosion products formed on titanium base materials exposed to WIPP Brine A at 150°C have been analyzed by obtaining electron diffraction patterns of oxide films which were selected from various positions on the crevice surface. The crevice corrosion products for CP titanium and TiCode-12 are mainly an anatase form of  $TiO_2$ . Both materials also showed trace amounts of  $Ti_3O_5$ . The intensity of the  $Ti_3O_5$  peak in the diffraction pattern is stronger in CP titanium than in TiCode-12. More  $Ti_3O_5$  is formed in the center of the crevice. From the study, it seems that the color differences of oxides inside the crevice are mainly due to optical interference colors caused by varying film thickness.

The open-circuit corrosion potential behavior of CP titanium and TiCode-12 has been examined in acidified Brine A at 80°C. To reduce the potential effect of oxidizing impurities in test media these solutions were pre-electrolyzed. Both materials show breakdown of the passive film. TiCode-12 reaches a quasi steady state potential more rapidly than CP titanium. Breakdown of the passive film is attributed to the high chloride concentration with Ni being preferentially dissolved.

Single-edged-notched tensile specimens have been used to obtain the apparent stress intensity factors at 2% crack extension in hydrogenated TiCode-12 with hydrogen concentrations up to 10,900 ppm. For high hydrogen levels the apparent stress intensity factor dropped roughly by a factor of 10 compared to nonhydrogenated TiCode-12. Fractographs show both alpha phase crystallographic fracture and alpha-beta interface cracking. These fractographs indicate that the formation of hydride is responsible for crack initiation for hydrogen concentrations above 5000 ppm.

Notched c-rings of CP titanium and TiCode-12 have been loaded and immersed in acidified Brine A to test for stress corrosion cracking susceptibility. These tests are presently under way.

## FIGURES

1.	TiCode-12 Specimens From Which TEM Samples Were Prepared . . . . .	2
2.	The TEM Microstructure of the Yellow Film Formed in Position 1 Showing Pointed and Block-Shaped Crystals. . . . .	2
3.	SEM Photomicrograph of the Violet Film Formed Inside the Crevice of TiCode-12. . . . .	3
4.	The TEM Microstructure of the Blue Film Formed Inside the Crevice of TiCode-12 . . . . .	4
5.	CP Titanium Crevice Corrosion Specimen From Which TEM Samples Were Prepared. . . . .	5
6.	Carbon Replica of an Anatase Form of TiO <sub>2</sub> Formed Inside the Crevice of CP Titanium . . . . .	6
7a.	Electron Diffraction Pattern From the Violet Film Inside the TiCode-12 Crevice . . . . .	7
7b.	Electron Diffraction Pattern From the Blue Film Formed on CP Titanium by Gas Flame Oxidation in Air. . . . .	7
8.	X-Ray Diffraction Pattern of the Crevice Corrosion Product of CP Titanium . . . . .	9
9.	Open-Circuit Corrosion Potential of CP Titanium in Acidified Brine A at 80°C. . . . .	11
10.	Open-Circuit Corrosion Potential of TiCode-12 in Acidified Brine A at 80°C. . . . .	12
11.	Ductile Fracture of TiCode-12 With a Hydrogen Concentration of 100 ppm . . . . .	15
12.	Hydrogen Induced Interface Facets Formed by Brittle Interface Cracking of TiCode-12 With Hydrogen Above 5000 ppm . . . . .	17
13.	Hydrogen Induced Interface Facets Observed After Rotation of the Sample Position in Figure 12 . . . . .	17
14.	Hydrogen Induced Intermittent Brittle Crack Propagation in a Grain of TiCode-12 with Hydrogen Concentration Above 5000 ppm. Note Secondary Interface Cracking in the Center . . . . .	18

#### ACKNOWLEDGMENT

Our thanks go to G. Spira and R. Jones for their general technical assistance and P. Klotz and J. Forrest for their work on chemical analyses. We wish to express our sincere appreciation to Ms. S. M. Moore and Ms. G. F. Searles for their efforts and patience in the typing and preparation of this report.

## 1. INTRODUCTION

The current program was initiated to determine potential corrosion failure modes in TiCode-12 high level waste container material exposed to prototypic repository conditions. A basic goal was to elucidate the mechanism by which failure occurs and to develop means of extrapolating short term test data to the prediction of very long term container behavior. Work to date in this program has shown that crevice corrosion is a possible failure mode in TiCode-12. This is the first observation that has been made of this type of corrosion in a simulated repository brine environment. Thus, a major part of the BNL effort is directed to finding conditions under which it occurs, determining the precise mechanism of failure, and to evaluating whether the occurrence of long term crevice attack will compromise container integrity. Efforts in this quarter have been concentrated on the crevice corrosion and hydrogen embrittlement of TiCode-12 and CP titanium. Electrochemical work in acidified brines has also been performed to aid in understanding the corrosion of these materials in the crevice environment.

## 2. CREVICE CORROSION

### 2.1 Identification of the Crevice Corrosion Product

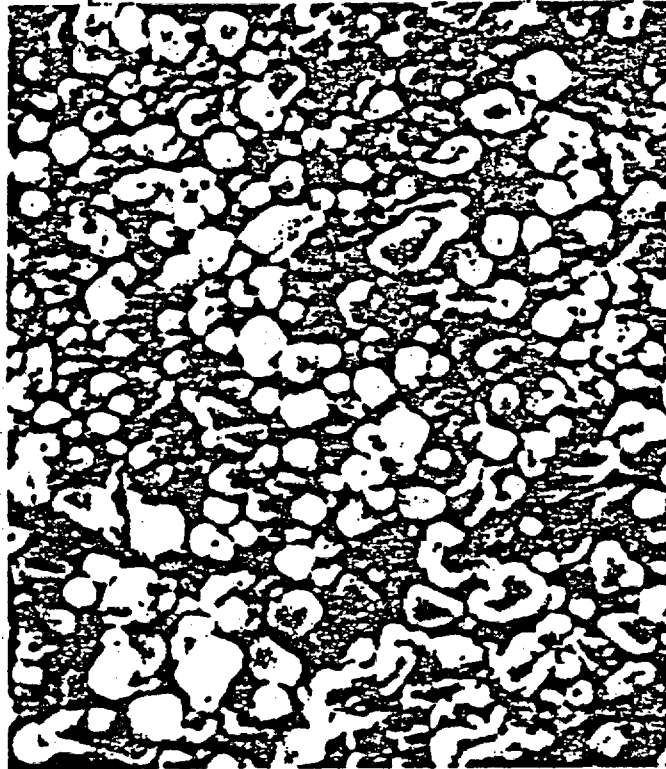
As reported earlier by BNL,<sup>1</sup> it was possible to identify the corrosion product formed in the crevices of TiCode-12 and CP titanium with an electron diffraction technique utilizing TEM (Transmission Electron Microscopy). In this quarter, more work was conducted to obtain additional data for identifying the corrosion products. In the current work, the TEM diffraction samples were selected from different colored parts of the film inside the crevice. This enabled us to study crevice corrosion as a function of the distance from the crevice perimeter and to determine whether the colors are caused by optical interference or by different oxide phases.

#### 2.1.1 TiCode-12

As shown in Figure 1, three samples taken from films with different colors were prepared. The yellow film (position 1, Figure 1) showed crystals with different shapes including pointed and block shaped crystals (Figure 2). All the diffraction rings for the crystals match the peaks for the anatase form of  $\text{TiO}_2$ , except one peak at  $d = 1.76\text{\AA}$ .

The violet film (position 2, Figure 1) showed mostly block shaped crystals with a few pointed crystals. The diffraction patterns show strong anatase ( $\text{TiO}_2$ ) peaks, with two extra weak peaks at  $d \sim 2.13$  and  $1.75\text{\AA}$ . Figure 3 is an SEM (Scanning Electron Microscopy) photomicrograph of this violet film.

The blue film (position 3, Figure 1) consisted mostly of block shaped crystals with almost no pointed crystals, as shown in Figure 4. All the strong peaks were identified as those from anatase ( $\text{TiO}_2$ ). Additional peaks ( $d \sim 2.85, 2.15, 2.03, 1.77, \text{ and } 1.41\text{\AA}$ ) were observed although they were very weak.



0.5  $\mu$

Figure 3. SEM photomicrograph of the violet film formed inside the crevice of TiCode-12.

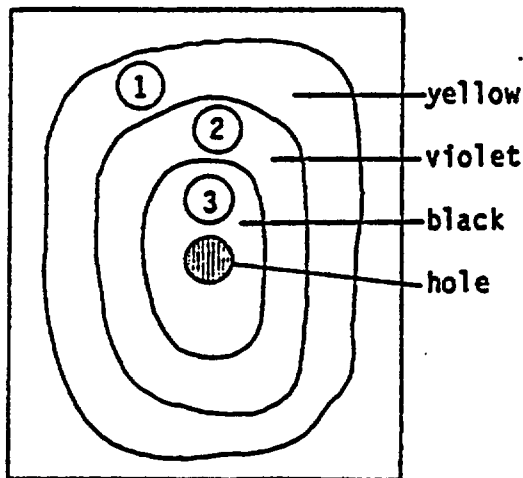


Figure 5. CP titanium crevice corrosion specimen from which TEM samples were prepared. 1, 2, and 3 denote the locations of the areas studied. The crevice specimen was immersed in Brine A at 150°C for 12 weeks.

### 2.1.2 CP Titanium

As shown in Figure 5, three samples with different colors were prepared from crevice regions. The yellow film (position 1, Figure 5) shows all the diffraction peaks of anatase with one very weak peak at  $d = 1.75\text{\AA}$ . The crystals do not have definite shapes, but are aggregates of small crystallites.

The diffraction pattern of the violet film showed all the peaks expected for anatase. The additional peaks were much stronger than those from TiCode-12 samples, and were more numerous. Figure 6 shows a carbon replica of the anatase crystals.

The black film shows strong extra peaks in addition to anatase peaks, at  $d \sim 4.49, 2.91, 2.78$  (band),  $2.16, 1.76,$  and  $1.42\text{\AA}$ . It was found that all the extra peaks for the TiCode-12 samples are in fact part of this set for CP titanium. This extra peak set matched best the  $\text{Ti}_3\text{O}_5$  diffraction pattern.

To compare the difference between the oxides present in the crevices and an air-formed oxide, an oxide film was formed in air on CP titanium using a gas flame. Electron diffraction patterns obtained from this film accurately matched those of the rutile form of  $\text{TiO}_2$ . The electron diffraction patterns from the crevice corrosion product and the air-formed oxide film are compared in Figures 7a and 7b. The two patterns are distinctly different. It is interesting to note that there was no trace of the rutile form of  $\text{TiO}_2$  inside the crevices of CP titanium or TiCode-12 exposed to brine.

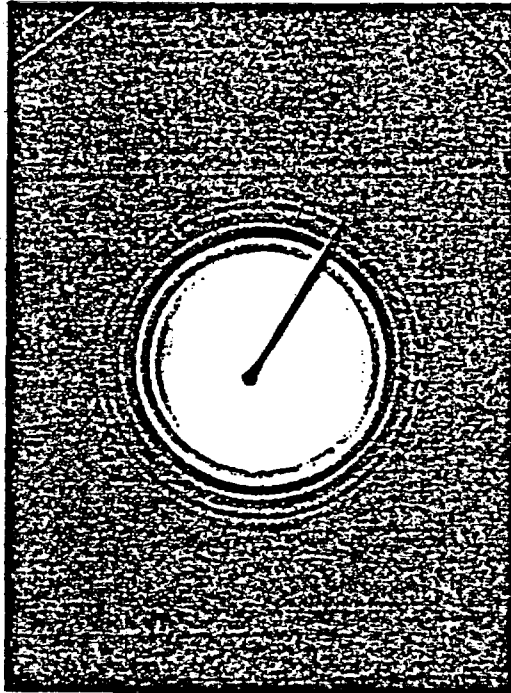


Figure 7a. Electron diffraction pattern from the violet film inside the TiCode-12 crevice.

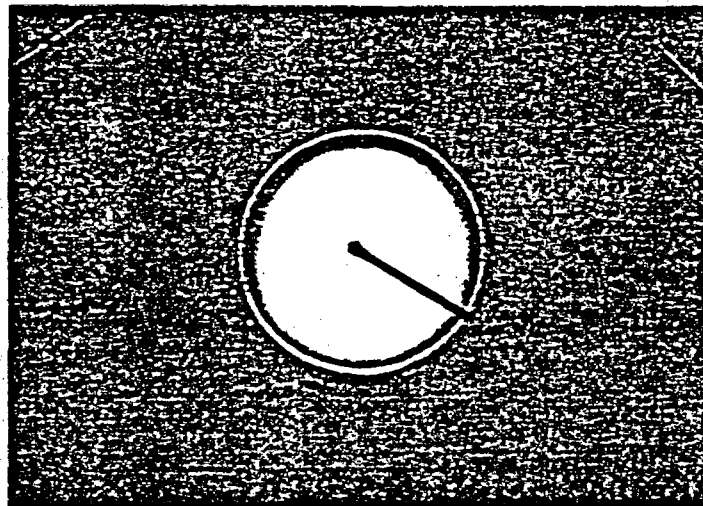


Figure 7b. Electron diffraction pattern from the blue film formed on CP titanium by gas flame oxidation in air.

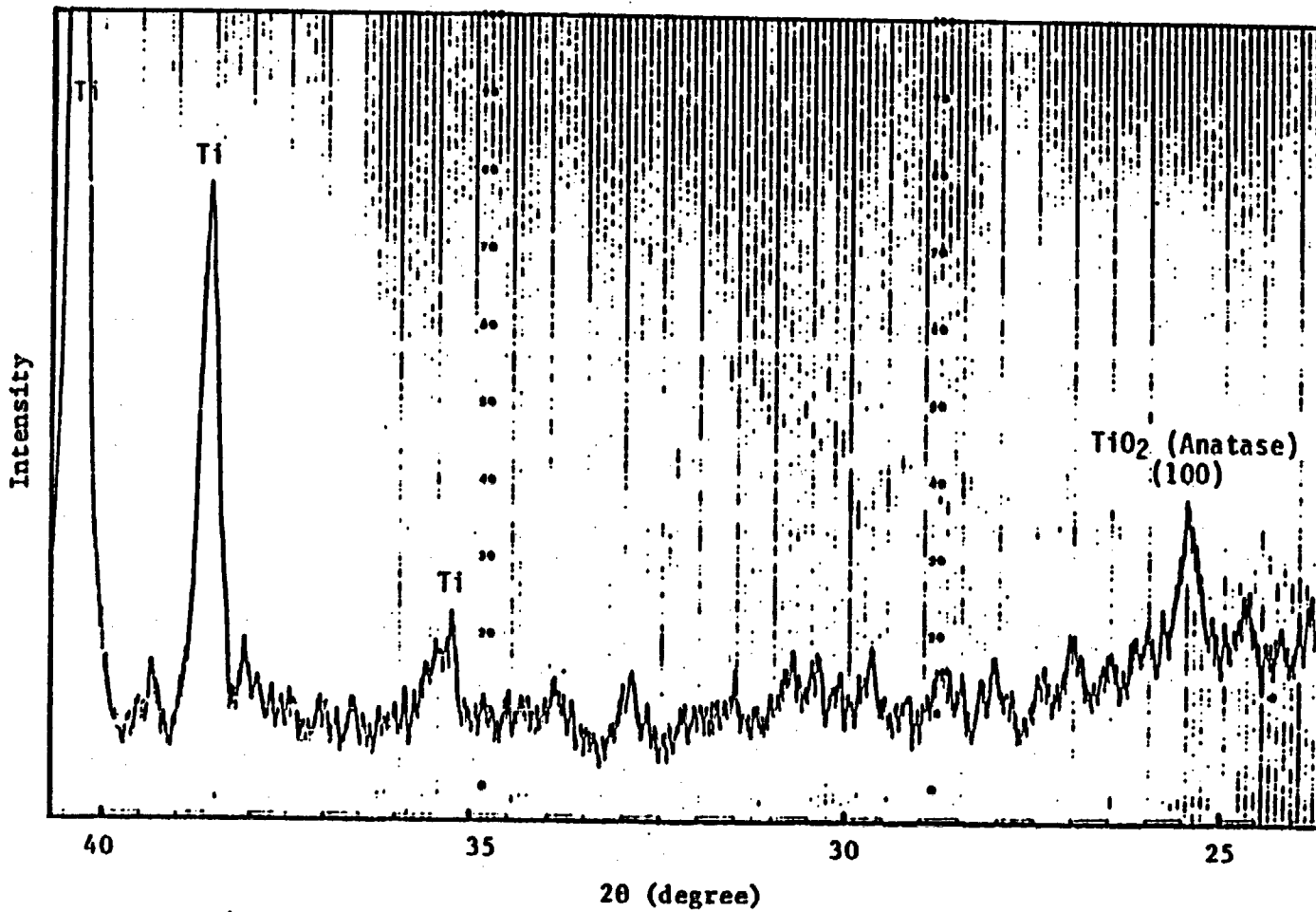


Figure 8. X-ray diffraction pattern of the crevice corrosion product of CP titanium.

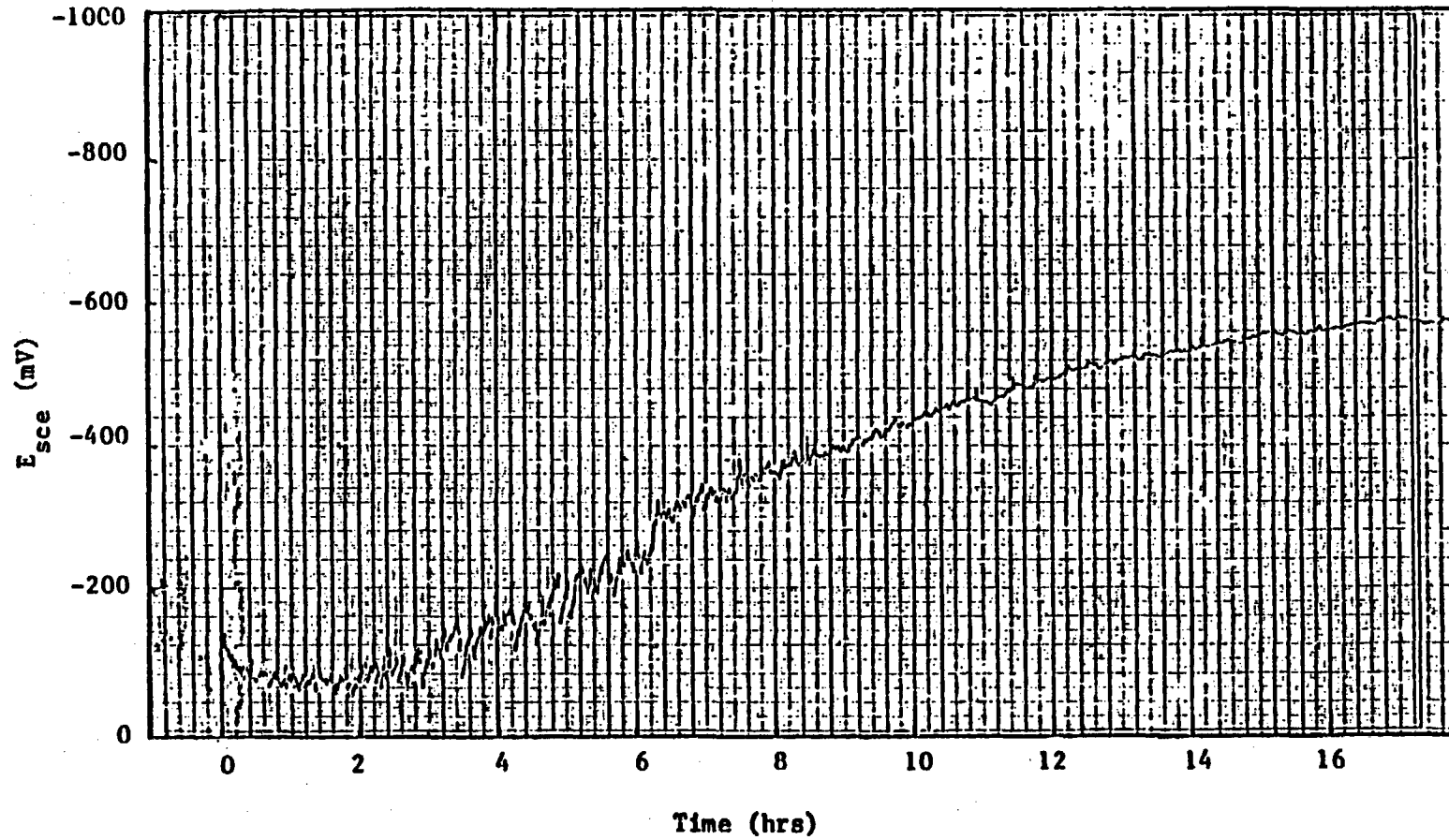


Figure 9. Open-circuit corrosion potential of CP titanium in acidified Brine A at 80°C.

Kelly's model<sup>6</sup> whereby passivation of an active surface is achieved by attaining some critical concentration of Ti(IV) ions, the present results for titanium in acidified brine could be considered in terms of a higher chloride/halide concentration necessitating a higher concentration of Ti(IV) ions to be present in solution before the surface is passivated.

The free corrosion potential of CP titanium suggests that it was initially in a passive state ( $E \sim -120$  mV sce, Figure 9) whereas TiCode-12 was not ( $E \sim -340$  mV sce, Figure 10). After approximately two-hours' immersion the passive behavior of the CP titanium surface appears to change in that the potential became more cathodic and fluctuated until  $E$  was  $\sim -300$  mV sce (Figure 9). The fluctuations probably indicate the ability of bulk impurities in the metal (e.g., Fe) surface to maintain passivation, but which are themselves cyclically depleted and enriched in the surface by dissolution. As film breakdown continues, the facility with which the bulk impurities can maintain passivation is reduced and the potential continues to fall until  $E \sim -300$  mV sce. In this potential range, the oxide film is reduced to a monolayer, according to Kelly.<sup>6</sup> The rapid decrease in potential at this point reported for high purity titanium ( $\text{pH} = 0$ ,  $[\text{Cl}^-] = 1$  M) by Kelly<sup>6</sup> is not observed here and may be due to the continued influence of the bulk impurities.

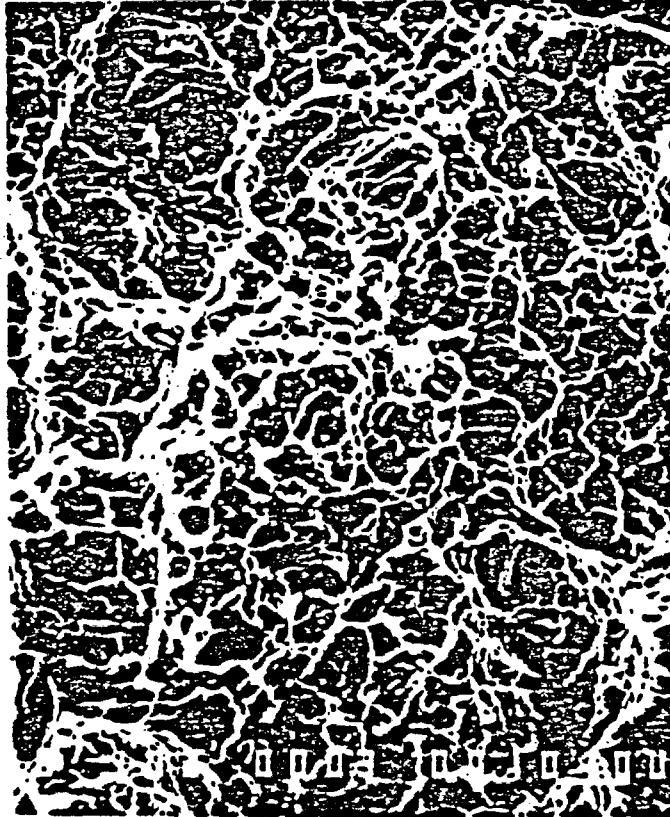
With continued immersion, the potential decreased linearly at an approximate rate of 34 mV per hour. After about 17 hours, it reached a "steady state" value of  $E \sim -620$  mV sce. This potential is similar to the open circuit potential attained by CP titanium under similar conditions following mechanical removal of the oxide (allowing for the difference in  $[\text{Cl}^-]$ ).<sup>1</sup> In fact, this potential  $\sim -620$  mV sce is very close to the potential shown by both Griess<sup>4</sup> and Kelly<sup>6</sup> at  $\text{pH} = 1$  and  $[\text{Cl}^-] = 1$  M to be that associated with the maximum corrosion rate and is independent of temperature.

The observations for TiCode-12 require further analysis. Previously it was reported that for similar conditions but lower  $\text{Cl}^-$  concentration ( $[\text{Cl}^-] = 1$  M) an abraded TiCode-12 surface attained a potential of approximately  $-400$  mV sce after approximately 83 minutes.<sup>1</sup> After the same time the o/c potential of TiCode-12 in acidified brine reaches approximately the same potential but at this point fluctuations in the potential are noted (Figure 10). It is not considered that these fluctuations are due to the same source (i.e., bulk impurities such as Fe) as in the case of CP titanium since the potential is considerably more cathodic and the fluctuations are much more rapid. Reference to work by Griess<sup>4</sup> reveals that a Ti-1% Ni-1% Mo alloy also exhibited essentially similar potential cycling over a time period of approximately 20 minutes. In this work, the time period was an order of magnitude shorter. Also, the fluctuation ranges from  $-315$  mV sce to  $-470$  mV sce in Griess'<sup>4</sup> work while the present study shows the average fluctuations varied from  $-550$  mV sce to  $-480$  mV sce, i.e., remaining more or less active. Reference to thermodynamic data allows some pertinent comments to be made regarding this fluctuation behavior of TiCode-12. In the potential range covered by the fluctuations, dissolution of Mo could be expected to be appreciably less than in the case of Ni, after considering the Pourbaix diagrams for Ni and Mo.<sup>7</sup> Further, in the case of stainless steel containing Mo, the mechanism of crevice corrosion inhibition in acidic chloride environments is

Table 1

The Apparent Stress Intensity Factor at Crack Initiation  
at Three Hydrogen Concentration Levels

Hydrogen Concentration (ppm)	100	6560	10900
$K_Q$ (MPa $\sqrt{m}$ )	45.4	4.5	5.8



10  $\mu$

Figure 11. Ductile fracture of TiCode-12 with a hydrogen concentration of 100 ppm.

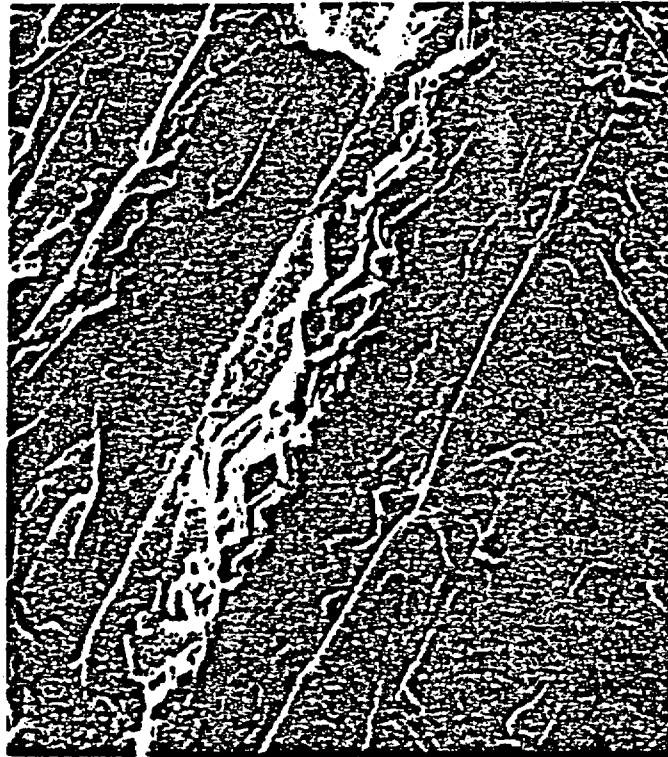


Figure 12. Hydrogen induced interface facets formed by brittle interface cracking of TiCode-12 with hydrogen above 5000-ppm.

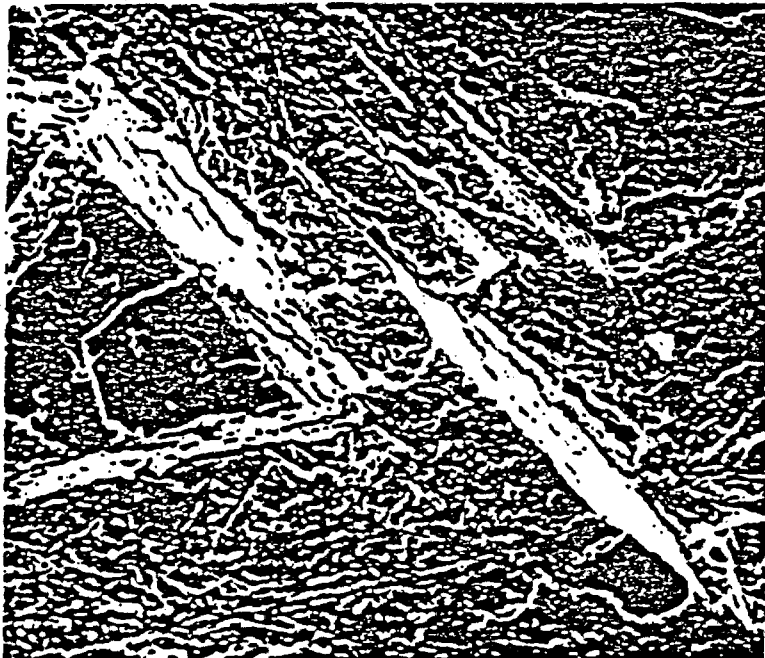


Figure 13. Hydrogen induced interface facets observed after rotation of the sample position in Figure 12.



10  $\mu$

Figure 16. Fracture surface of TiCode-12 with hydrogen concentration above 5000 ppm showing crystallographic fracture, magnification 1000X.



50  $\mu$

Figure 17. Fracture surface of TiCode-12 with hydrogen concentration above 5000 ppm showing crystallographic fracture, magnification 500X.

13. D. A. Meyn, "Effect of Hydrogen Content on Inert Environment Sustained Load Crack Propagation Mechanisms of Ti-6Al-4V," in Environmental Degradation of Engineering Materials in Aggressive Environments, M. R. Louthan, Jr., R. P. McNitt, and R. D. Sission, Jr., Eds, VPI, Virginia, 1981.
14. G. H. Koch, A. J. Bursle, R. Liu, and E. N. Pugh, "A Comparison of Gaseous Hydrogen Embrittlement, Slow-Strain-Rate Hydrogen Embrittlement, and Stress-Corrosion Cracking in Ti-8Al-1Mo-1V," Met. Trans. A. 12A, 1823 (1981).
15. D. A. Meyn, "Effect of Hydrogen on Fracture and Inert-Environment Sustained Load Cracking; Resistance of Alpha-Beta Titanium Alloys," Met. Trans. A. 5, 319 (1974).
16. D. A. Meyn and G. Sandoz, Met. Trans. 245, 1253 (1969).
17. M. J. Blackburn and J. C. Williams, Fundamental Aspects of Stress-Corrosion Cracking, p. 620, NACE, Houston, 1969.
18. N. R. Moody and W. W. Gerberich, "Hydrogen Induced Slow Crack Growth in Ti-6Al-6V-2Sn," Met. Trans. A 11A, 973 (1980).
19. D. A. Meyn, paper presented at TMS-AIME Fall Meeting in Niagara Falls, New York, September 1976.

NUREG/CR-2317  
BNL-NUREG-51449  
VOL. 1, NO. 3

# **CONTAINER ASSESSMENT — CORROSION STUDY OF HLW CONTAINER MATERIALS**

**QUARTERLY PROGRESS REPORT  
JULY — SEPTEMBER 1981**

**T.M. Ahn and P. Soo  
Principal Investigators**

**Contributors:  
B.S. Lee, J. Woodward  
R.C. Newman, and S. Aronson**

**Date Published — January 1982**

**PREPARED BY THE NUCLEAR WASTE MANAGEMENT DIVISION  
DONALD G. SCHWEITZER, HEAD  
DEPARTMENT OF NUCLEAR ENERGY, BROOKHAVEN NATIONAL LABORATORY  
UPTON, NEW YORK 11973**

**Prepared for the United States Nuclear Regulatory Commission  
Office of Nuclear Regulatory Research  
Under Contract No. DE-AC02-76CH00016  
Fin No. A-8237**

NUREG/CR-2317  
BNL-NUREG-51449  
Vol. 1, No. 3  
AN, WH

# **CONTAINER ASSESSMENT — CORROSION STUDY OF HLW CONTAINER MATERIALS**

**QUARTERLY PROGRESS REPORT  
JULY — SEPTEMBER 1981**

**T.M. Ahn and P. Soo  
Principal Investigators**

**Contributors:  
B.S. Lee, J. Woodward  
R.C. Newman, and S. Aronson**

**Manuscript Completed — November 1981  
Date Published — January 1982**

**PREPARED BY THE NUCLEAR WASTE MANAGEMENT DIVISION  
DONALD G. SCHWEITZER, HEAD  
DEPARTMENT OF NUCLEAR ENERGY, BROOKHAVEN NATIONAL LABORATORY  
UPTON, NEW YORK 11973**

**PREPARED FOR THE UNITED STATES NUCLEAR REGULATORY COMMISSION  
OFFICE OF NUCLEAR REGULATORY RESEARCH  
UNDER CONTRACT NO. DE-AC02-76CH00016  
FIN NO. A-3237**

## NOTICE

This report was prepared as an account of work sponsored by an agency of the United States Government. Neither the United States Government nor any agency thereof, or any of their employees, makes any warranty, expressed or implied, or assumes any legal liability or responsibility for any third party's use, or the results of such use, of any information, apparatus, product or process disclosed in this report, or represents that its use by such third party would not infringe privately owned rights.

The views expressed in this report are not necessarily those of the U.S. Nuclear Regulatory Commission.

Available from  
GPO Sales Program  
Division of Technical Information and Document Control  
U.S. Nuclear Regulatory Commission  
Washington, D.C. 20555  
and  
National Technical Information Service  
Springfield, Virginia 22161

## ABSTRACT

Work has been started on the corrosion and hydrogen embrittlement behavior of commercially pure titanium (ASTM Grade 2), TiCode-12 (ASTM Grade 12), and OFHC copper, which are primary candidate materials for high level waste containers. The test environment used is a simulated brine solution typical of bedded salt at 150°C or room temperature. The immersion test results for these materials are in reasonable agreement with previous screening test results of Sandia National Laboratory; electron beam welded titanium and TiCode-12 samples show higher corrosion rates than the non-welded samples.

To understand the difference between titanium and TiCode-12 in uniform and crevice corrosion, electrochemical tests were performed. While the initial repassivation behavior is similar in terms of charge density transfer after scratching tests in 1 M HCl solution at 80°C, titanium shows an active peak in polarization curves in brine at room temperature while TiCode-12 does not. Also, the open circuit corrosion potential of TiCode-12 is about 300 mV more anodic than that of titanium in 0.1 M HCl plus 0.9 M KCl solution at 85°C.

In the immersion tests on mechanically-creviced titanium, a major crevice corrosion product is observed which has various colors and was identified by Transmission Electron Microscopy to be a mixture of  $TiO_2$  and other low oxides such as  $Ti_2O_3$  and  $TiO$ . The crevice region of TiCode-12 shows a color change at 150°C with a thicker film forming at 200°C. The correlation of electrochemistry and immersion tests is under study. Sulfur introduced in a crevice simulation test on copper has been shown to cause attack. Copper, in the absence of sulfur, however, shows no visible crevice corrosion. As an aid to understanding uniform and crevice corrosion results, potential-pH diagrams are being constructed.

Slow strain rate embrittlement and impact embrittlement have been observed in cathodically hydrogen charged commercially pure titanium and TiCode-12 in tension and buckling tests. C-ring and U-bend specimens of titanium and TiCode-12 have been designed and a slow strain rate test machine is being built to study stress corrosion cracking. Alternating Current Impedance and Scanning Reference Electrode Techniques are ready for pitting studies.

For the study of radiation-induced corrosion, an irradiation cell was set up in the gamma pool to estimate quantitatively the oxidants as well as hydrogen produced by the gamma radiation in the brine solutions.

CONTENTS

ABSTRACT . . . . .	iii
CONTENTS . . . . .	v
TABLES . . . . .	vi
FIGURES . . . . .	vii
ACKNOWLEDGEMENTS . . . . .	viii
1. INTRODUCTION . . . . .	1
2. MATERIALS AND SOLUTIONS. . . . .	1
3. UNIFORM CORROSION. . . . .	4
4. ELECTROCHEMISTRY . . . . .	4
5. CREVICE CORROSION. . . . .	11
6. DETERMINATION OF POTENTIAL-pH DIAGRAMS FOR Cu, Pb, AND Ti IN AQUEOUS SOLUTIONS WITH HIGH CHLORIDE CONTENT . . . . .	15
7. STRESS CORROSION AND PITTING CORROSION . . . . .	19
8. HYDROGEN EMBRITTLEMENT . . . . .	19
9. RADIATION EFFECTS. . . . .	23
10. REFERENCES . . . . .	25

TABLES -

1.	Compositions of Commercially Pure Titanium Grade 2 and TiCode-12 . . . . .	1
2.	Composition of Brine Solutions. . . . .	3
3.	Compositions of Rock Salt Saturated Solutions . . . . .	3
4.	Corrosion Rates of TiCode-12, EB TiCode-12, and EB Titanium at 150°C . . . . .	5
5.	Ions Considered in the Potential-pH Diagram . . . . .	16

## FIGURES

1.	Microstructure of Alpha and Beta Phases of TiCode-12. . . . .	2
2.	Capsule Test Design for Uniform and Crevice Corrosion Testing . . . . .	4
3.	Kinetics of Uniform Corrosion for Copper at 150°C . . . . .	5
4.	Schematic Diagram of Polarization Curves for Commercially Pure Titanium in Chloride Solution. . . . .	6
5.	A. The Polarization Curves for Pure Titanium Grade 2 and TiCode-12 in Brine A at Room Temperature. . . . .	7
	B. The Polarization Curves for Pure Titanium Grade 2 and TiCode-12 in Brine B at Room Temperature. . . . .	8
6.	The Open-circuit Potential Transient of Titanium and TiCode-12 at 85°C in 0.1 M HCl + 0.9 M KCl at 85°C. . . . .	10
7.	Simulated Crevice by Bolt-Joining Two Coupons . . . . .	11
8.	Corrosion Product in the Crevice of Titanium. . . . .	12
9.	Corrosion Product in the Crevice of TiCode-12 and EB TiCode-12. . . . .	13
10.	TEM Microstructure of Lower Oxide in the Crevice Region for Titanium. . . . .	14
11.	Sulfur Attack on Copper Observed at the Interface of Cu/Rubber Band . . . . .	16
12.	Potential-pH Equilibrium Diagram for the System Copper-Brine A and B at 25°C. . . . .	17
13.	Potential-pH Equilibrium Diagram for the System Lead-Brine A and B in the absence of HCO <sub>3</sub> at 25°C . . . . .	18
14.	C-ring and U-bend specimens for Stress Corrosion Testing. . . . .	19
15.	Fractograph of Slow Strain Rate Embrittled TiCode-12. . . . .	21
16.	Fractograph of Nonhydrogenated TiCode-12. . . . .	21
17.	Buckling Test Result on Hydrogenated and Nonhydrogenated TiCode-12 . . . . .	22
18.	Fractograph of Impact Embrittled TiCode-12. . . . .	22

## ACKNOWLEDGEMENTS

Our thanks go to G. Spira and R. Jones for their general technical assistance, R. Sabatini for his contributions in the electron metallography, and P. Klotz and J. Forrest for their work on chemical analyses. We wish to express our sincere appreciation to Ms. S. M. Moore and Ms. G. F. Searles for their efforts and patience in the preparation of this report.

## 1. INTRODUCTION

Initial work is presented on the corrosion and hydrogen embrittlement behavior of commercially pure titanium (ASTM Grade 2), TiCode-12 (ASTM Grade 12) and OFHC copper, which are primary candidate materials selected by DOE<sup>1-4</sup> and foreign countries for HLW containers.<sup>5-7</sup> A major aim of this program is to confirm that the container materials selected will withstand corrosion and hydrogen attack for extended periods. Following the outline of this program described in the last report,<sup>8</sup> the progress made in this quarter includes results in the areas of uniform corrosion, crevice corrosion and pitting corrosion, stress corrosion and hydrogen embrittlement, and radiation effects.

## 2. MATERIALS AND SOLUTIONS

Pure titanium (Grade 2) and TiCode-12 (Grade 12) plates and sheets were obtained from three different sources; RML, Timet, and Crucible. The nominal compositions and mill analyses are shown in Table 1. TiCode-12 was reanalyzed

Table 1  
Compositions of Pure Titanium Grade 2 and TiCode-12

Weight Percent	Ni	Mo	Fe	C	H	N	O	Ti
<u>Commercially Pure Titanium</u>								
Nominal Composition	--	--	0.30M*	0.10	0.015	0.03M	0.25	Bal.
25.4 mm Plate (RMI), (Mill Anal.)	--	--	0.02	0.01	0.0032	0.013	0.131	Bal.
0.5 mm Sheet (Crucible) (Mill Anal.)	--	--	0.09	0.02	0.0055	0.008	0.138	Bal.
<u>TiCode-12</u>								
Nominal Composition	0.80	0.30	0.3M	0.1M	0.015M	0.03M	0.25M	Bal.
19.1 mm Plate (Timet):								
(Mill Anal.)	0.74	0.29	0.14	0.012	0.01	0.01	0.13	Bal.
(BNL Anal.)	0.72	0.53	0.22	--	--	--	--	Bal.
0.9 mm Sheet (Timet):								
(Mill Anal.)	0.82	0.29	0.09	0.013	0.01	0.15	0.16	Bal.
(BNL Anal.)	0.71	0.60	0.12	--	--	--	--	Bal.
6.4 mm Plate (Timet):								
(BNL Anal.)	0.99	0.54	0.50	--	--	--	--	Bal.

\*M denotes the maximum

at BNL for confirmation and the results are included in Table 1. While titanium and copper are single phase, TiCode-12 is a two phase material composed of alpha and beta phases. Beta phase (light colored) is minor compared to alpha phase (Figure 1). OFHC (Oxygen Free High Conductivity) copper sheets were purchased from Newhaven Copper Mill.



—|—  
10 $\mu$

Figure 1. Microstructure of Alpha and Beta Phases of TiCode-12.

Brine solutions selected for this study were based on work done by Sandia<sup>2</sup> and are considered to simulate salt repository conditions. The concentrations of the major ions in the two solutions used are shown in Table 2. Brine A is a high Mg/K/Na chloride brine and is representative of water which might intrude into the proposed WIPP (Waste Isolation Pilot Plant) site by percolation through an overlying zone containing potash, and it is also considered tentatively representative of minute brine inclusions found in bedded-salt formations.<sup>9</sup> Brine B is a near-saturated, predominantly NaCl brine representative of dissolved, bedded salt at the 800 m level of the proposed WIPP site.<sup>9</sup>

Table 2

Compositions of Brine Solutions

Component	Concentration (ppm)	
	Brine A	Brine B
Na <sup>+1</sup>	42,000	115,000
K <sup>+1</sup>	30,000	15
Mg <sup>+2</sup>	35,000	10
Ca <sup>+2</sup>	600	900
Sr <sup>+2</sup>	5	15
Cl <sup>-1</sup>	190,000	175,000
SO <sub>4</sub> <sup>-2</sup>	3,500	3,500
I <sup>-1</sup>	10	10
HCO <sub>3</sub> <sup>-1</sup>	700	10
Br <sup>-1</sup>	400	400
BO <sub>3</sub>	1,200	10

Data taken from Reference 2.

To confirm the solution chemistry, a rock salt block was obtained from Sandia Laboratory. Deionized water was saturated with the rock salt at 100°C and the solution analyzed as shown in Table 3. The results of the analysis generally agree with composition of Brine B reported by Sandia.<sup>2</sup> Effort in this quarter was primarily concerned with studies using of Brine A.

Table 3

Compositions of Rock Salt Saturated Solutions

Ion	Solution 1* (ppm)	Solution 2* (ppm)
Na <sup>+1</sup>	120,000	120,000
Ca <sup>+2</sup>	827	1,230
Cl <sup>-1</sup>	168,000	176,000
SO <sub>4</sub> <sup>-2</sup>	4,320	7,110

\*Solutions 1 and 2 are made from two different portions of the rock salt.

### 3. UNIFORM CORROSION

Immersion tests were used to study uniform corrosion. Each coupon (1-cm x 2-cm) of sheet material was polished mechanically for nonwelded specimens and immersed in a Brine A quartz tube maintaining the ratio of solution volume to surface area at 20 ml/cm<sup>2</sup> <sup>10</sup> (Figure 2). Weld samples were cleaned by pickling in 5% HF-35% HNO<sub>3</sub> solution. The capsules were heated for various times at 150°C. This type of experiment is both economical and useful with no significant synergistic effect between capsule and coupon reported.<sup>11</sup>

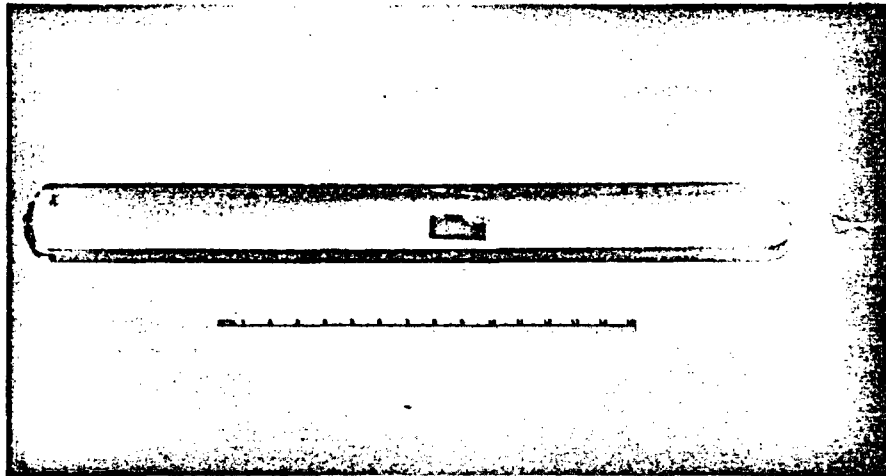


Figure 2. Capsule test design for uniform and crevice corrosion testing.

Figure 3 shows the weight loss of copper as a function of exposure. The results are in agreement with previous results.<sup>12</sup> Oxygen consumption and solubility limits are being analyzed to understand these results. Table 4 shows the corrosion rates of TiCode-12, EB (Electron Beam Weld) TiCode-12 and EB titanium. The result for TiCode-12 is in agreement with previous data.<sup>3</sup> Welded samples generally show higher weight losses compared with non-welded samples in the same environment.

### 4. ELECTROCHEMISTRY

To obtain more information on uniform corrosion and to study the relationship between the passivation characteristics and crevice corrosion of titanium

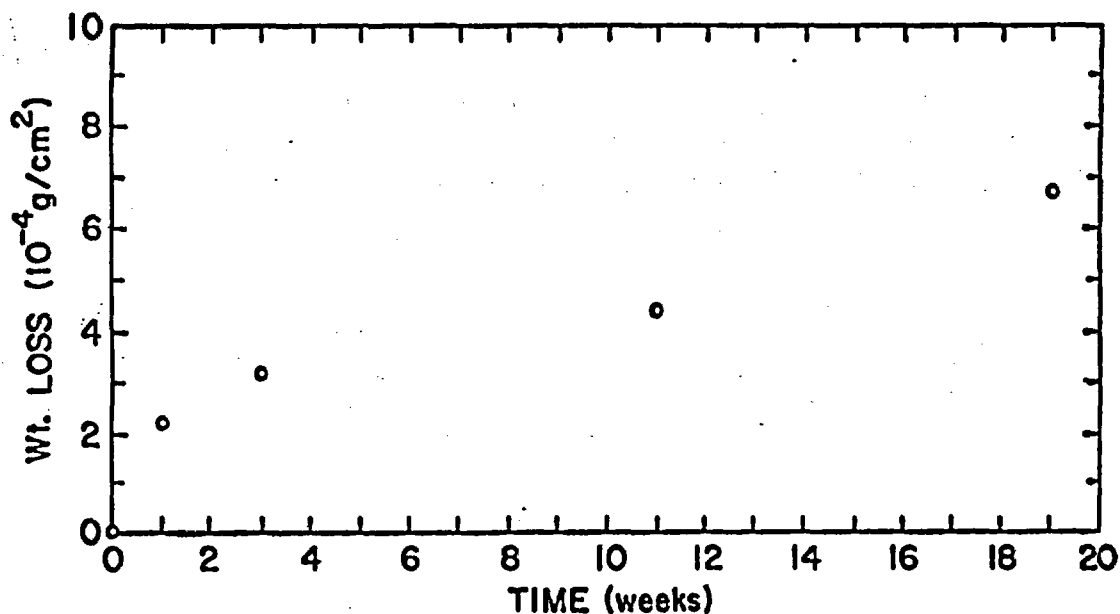


Figure 3. Kinetics of uniform corrosion for copper at 150°C.

Table 4

Corrosion Rates of TiCode-12, EB TiCode-12, and EB Titanium at 150°C

	Duration (Days)	Corrosion Rate ( $\mu\text{m}/\text{year}$ )
TiCode-12 (Non-welded)	75.8	1.70
TiCode-12 (Welded)	27.1	3.24
Titanium, Grade 2 (Welded)	27.1	4.42

and TiCode-12, three different electrochemical techniques were employed: (1) standard potentiodynamic polarization testing in brine solution at room temperature, (2) measurement of the charge density flowing through the specimen after removing the air-formed film in 1 M HCl solution at 80°C, and (3) measurement of the open circuit potential transient in deoxygenated 0.1 M HCl + 0.9 M KCl solution at 85°C.

The polarization curves were generated using an EG&G corrosion cell with graphite counter electrodes and a SCE (saturated calomel reference electrode).

Figure 4 shows a schematic diagram of polarization curves for commercially pure titanium in chloride<sup>13</sup> solution as a standard. At a scanning rate of 1 mV/sec, the polarization curves for pure titanium and TiCode-12 are different at room temperature (Figure 5). Titanium shows an active peak at  $\sim -770$  mV (SCE) while TiCode-12 does not.

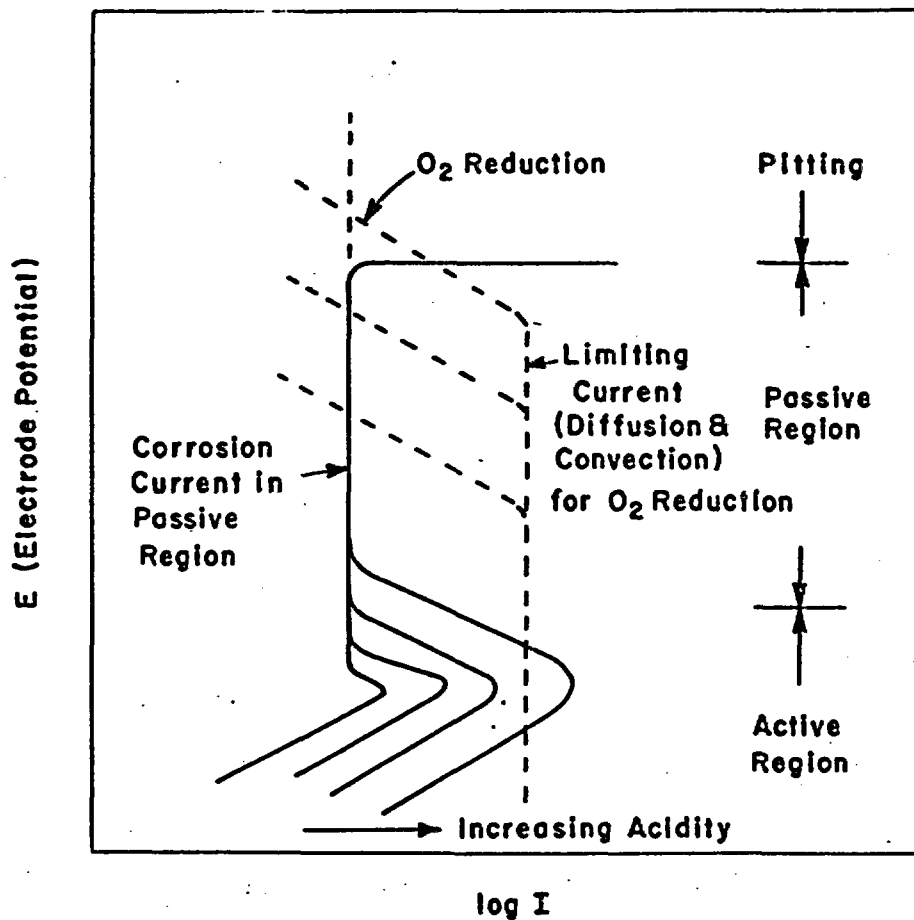


Figure 4. Schematic diagram of polarization curves for commercially pure titanium in chloride solution.<sup>13</sup>

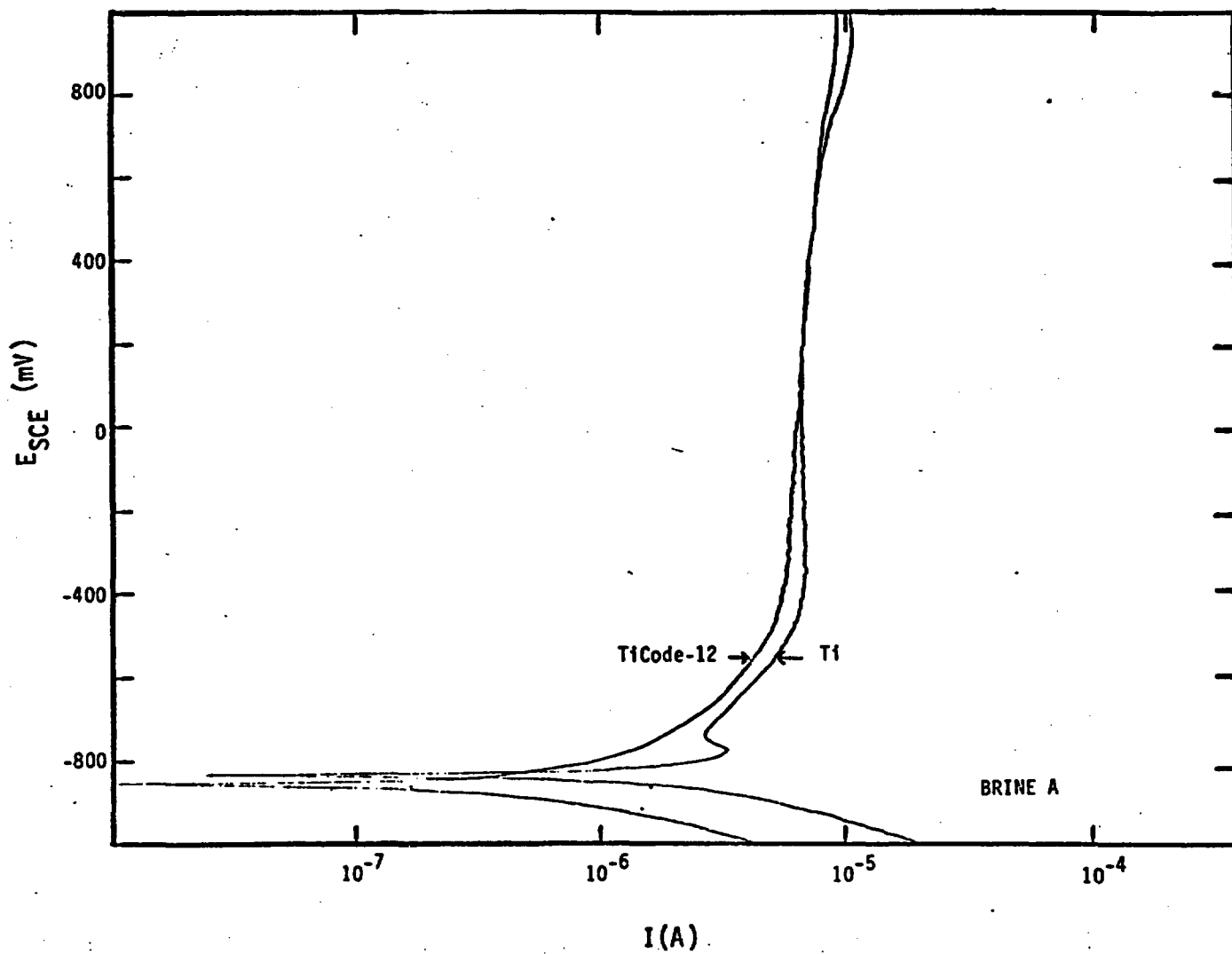


Figure 5A. The polarization curve for titanium Grade 2 and TiCode-12 in Brine A at room temperature.

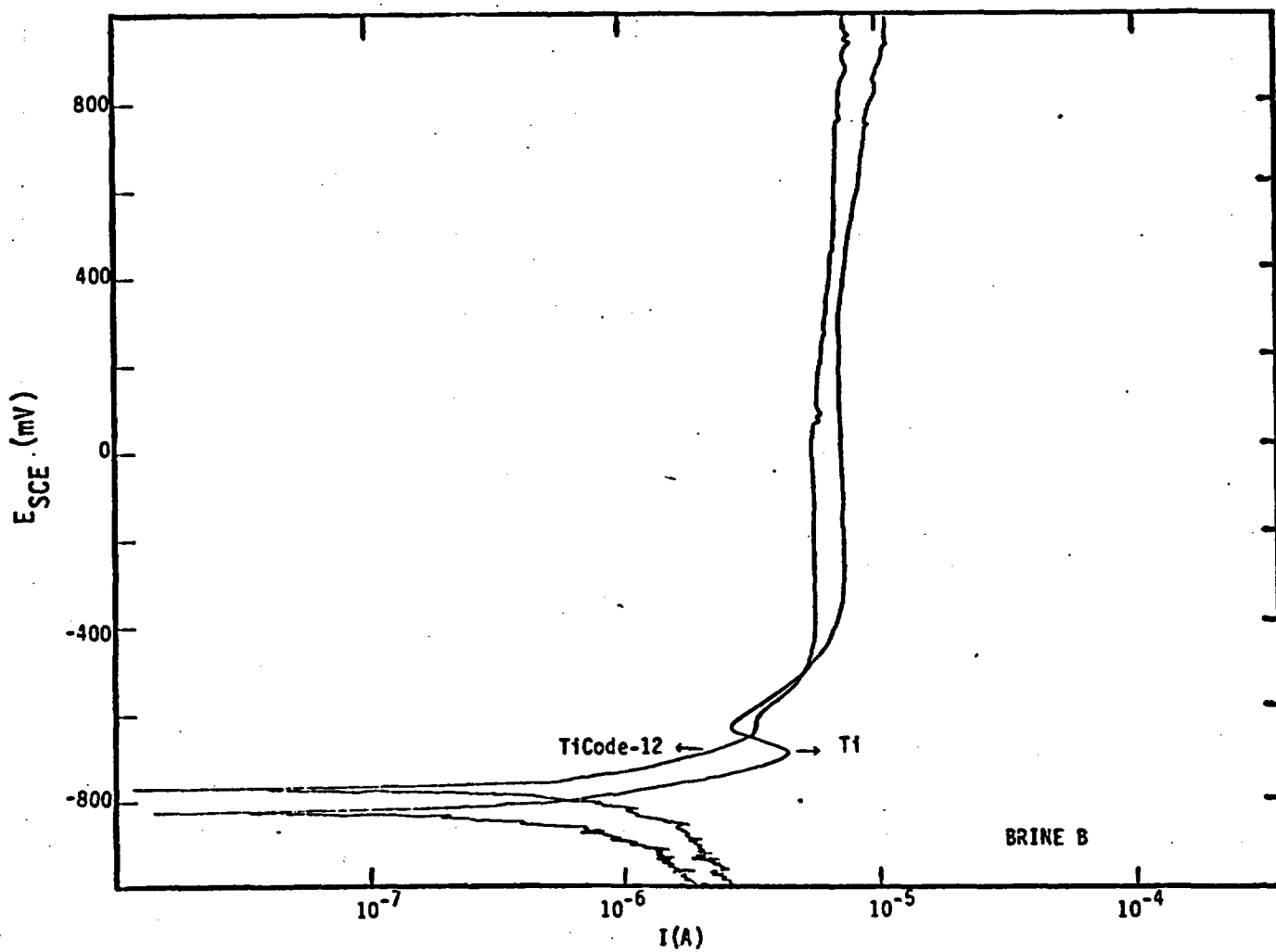


Figure 5B. The polarization curve for titanium Grade 2 and TiCode-12 in Brine B at room temperature.

Sandia<sup>2</sup> studied the polarization behavior of titanium and TiCode-12 in brine at higher temperatures up to 245°C and concluded that the only significant difference occurs at both 70°C and 245°C in the Cl<sub>2</sub> evolution reaction. It is believed that they could not observe the active peak for pure Ti because the surfaces of the specimens were covered with passive films. As soon as a polished specimen is exposed to the brine solution, the corrosion potential begins to move in a noble direction, which indicates the formation of a passive film. At higher temperatures, this passive film formation might be faster compared to lower temperatures, and consequently the active peak would not necessarily be observed in the polarization curve. There was no significant difference in the corrosion potentials of pure Ti and TiCode-12 in Brine A and B solutions at 25°C. Results indicate that at the same potential (at corrosion potential) TiCode-12 makes a passive film more easily and faster than pure Ti.

In order to understand corrosion in an acidic environment, which is expected in a crevice,<sup>14</sup> repassivation studies were initiated in 1 M HCl solution. Titanium and TiCode-12 specimens were fixed to the base of a Pyrex vessel using epoxy resin, and 1 M HCl added. A platinum counter electrode and SCE reference were used. A diamond tipped scribe, coated with plastic except for the tip, was used to scratch the surface at 80°C, with the potential controlled by a potentiostat. The resulting current transients were stored on a digital storage oscilloscope. The areas of the scratches were measured using width x length. Assuming a roughness factor of 1.5,<sup>15</sup> the current vs time transients were integrated to give the total excess charge (and therefore charge density) passed on the scratches.

The current transients observed at -530 mV (the active peak of titanium in 1 M HCl)<sup>16</sup> were very short, with >95% repassivation occurring within 100 ms of last diamond contact (the contact time was typically 50 ms). Values of the charge density  $q_s$  (microcoulombs/cm<sup>2</sup>) passed were as follows (from 5 scratches).

Titanium	$\frac{q_s, \mu\text{C}/\text{cm}^2}{420 \pm 100}$
TiCode-12	$400 \pm 100$

Thus, the two specimens behave essentially similarly. No noticeable differences in  $q_s$  were observed at potentials up to -250 mV (SCE) where it was still typically 400-500  $\mu\text{C}/\text{cm}^2$  and the specimens were passive at steady state. For a perfect polycrystalline titanium surface, 400  $\mu\text{C}/\text{cm}^2$  would represent about 2 electrons per surface atom, or a single complete monolayer of Ti(OH)<sub>2</sub>. This confirms Kelly's predictions.<sup>16</sup> It is hardly surprising that the primary passivation is the same for titanium and a highly dilute alloy such as TiCode-12. The reason the scratch test does not give values of  $q_s$  varying up to 800  $\mu\text{C}/\text{cm}^2$  (i.e., 1 monolayer Ti<sup>4+</sup>) is that the conversion of Ti<sup>2+</sup> to Ti<sup>4+</sup> in the monolayer is slow as pointed out by Kelly.<sup>16</sup>

Experiments were also performed in which the whole exposed surface of rotating titanium and TiCode-12 electrodes were abraded under a deoxygenated solution of 0.1 M HCl and 0.9 M KCl (pH 1). This solution is considered representative of a crevice corrosion environment.<sup>14</sup> Both open circuit and potentiostatic measurements were made up to 100°C. Figure 6 is an example of the open-circuit potential transient behavior of titanium and TiCode-12 at 85°C. At 50°C and above, TiCode-12 seemed to passivate spontaneously at open circuit ( $E \sim -400$  mV (SCE)), while titanium remained at a low, active potential ( $E \sim -700$  mV (SCE)).

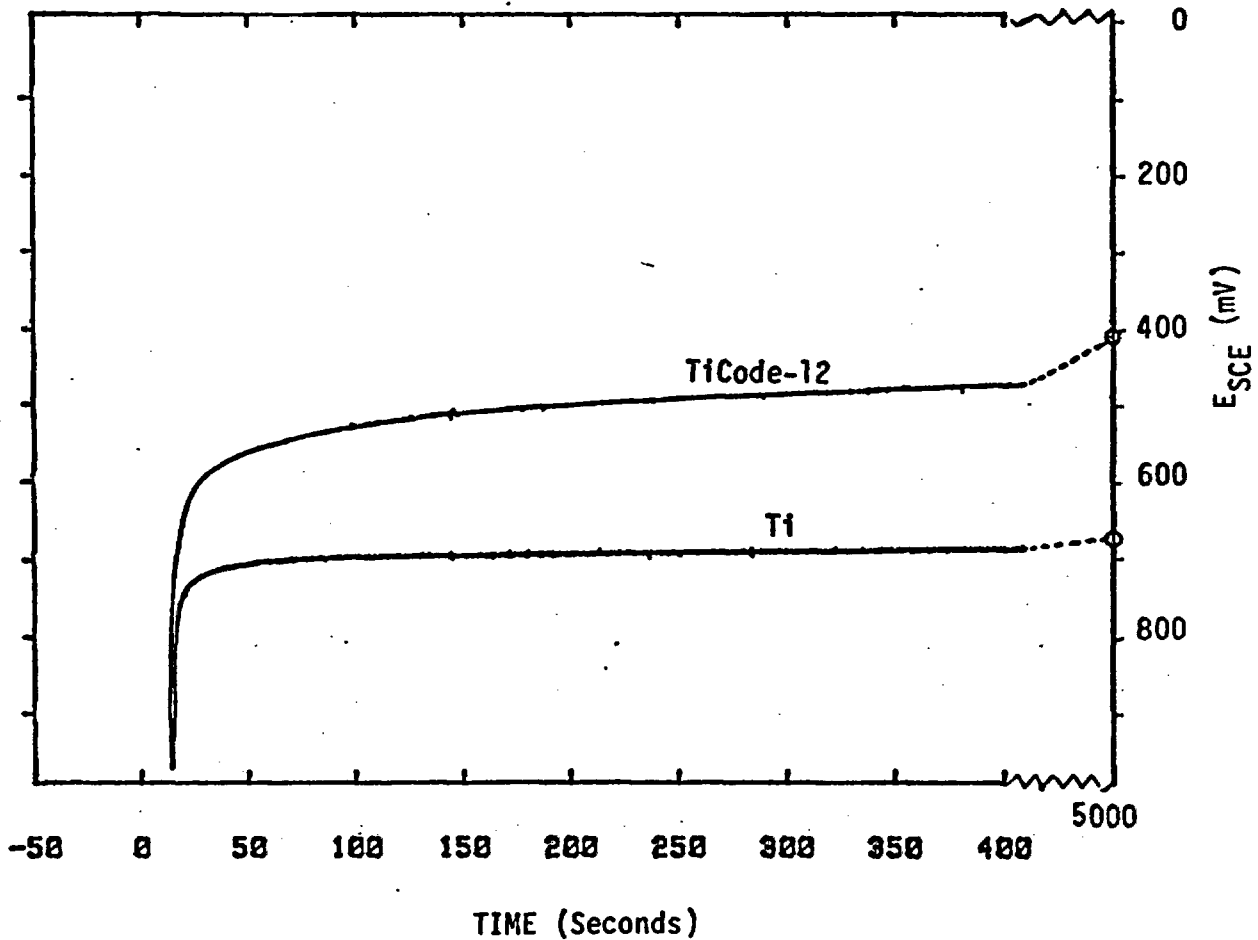


Figure 6. The open-circuit potential transient of Titanium and TiCode-12 at 85°C in 0.1 M HCl + 0.9 M KCl at 85°C.

The spontaneous repassivation of TiCode-12 is being confirmed. If this observation is correct, this may be the result of enhancement of the hydrogen ion reduction reaction by nickel. These studies in severe environments will be continued to gain an understanding of localized corrosion.

## 5. CREVICE CORROSION

Earlier results from Sandia showed that TiCode-12 does not show any signs of crevice corrosion while pure titanium experienced severe crevice corrosion.<sup>2</sup> This task was undertaken to investigate under what conditions TiCode-12 is susceptible or immune to crevice corrosion. An understanding of the mechanisms involved in the phenomena is also one of our objectives.

Titanium, TiCode-12 and EB TiCode-12 coupons were immersion-tested following the method described in the previous section on uniform corrosion. Titanium and TiCode-12 were mirror polished with 1 $\mu$  diamond paste and EB TiCode-12 was pickled to clean it. The crevice was simulated by joining two coupons with a nylon bolt through a hole made in the center of the coupons (Figure 7). The period of immersion was 12 weeks.

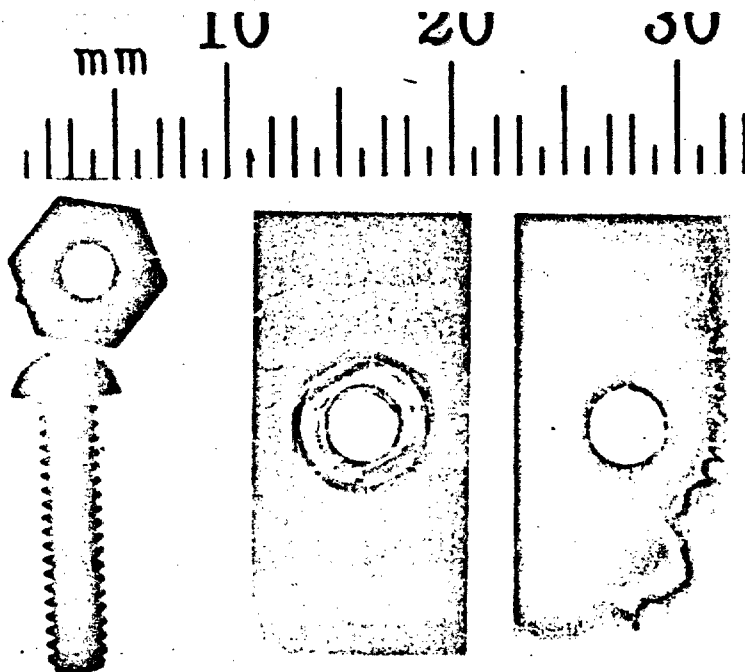


Figure 7. Simulated crevice by bolt-joining two coupons.

Titanium showed a black corrosion product in the center of the crevice after about two weeks with various colors (yellow, blue, and purple) in the crevice region away from the central hole (Figure 8). Results for various times

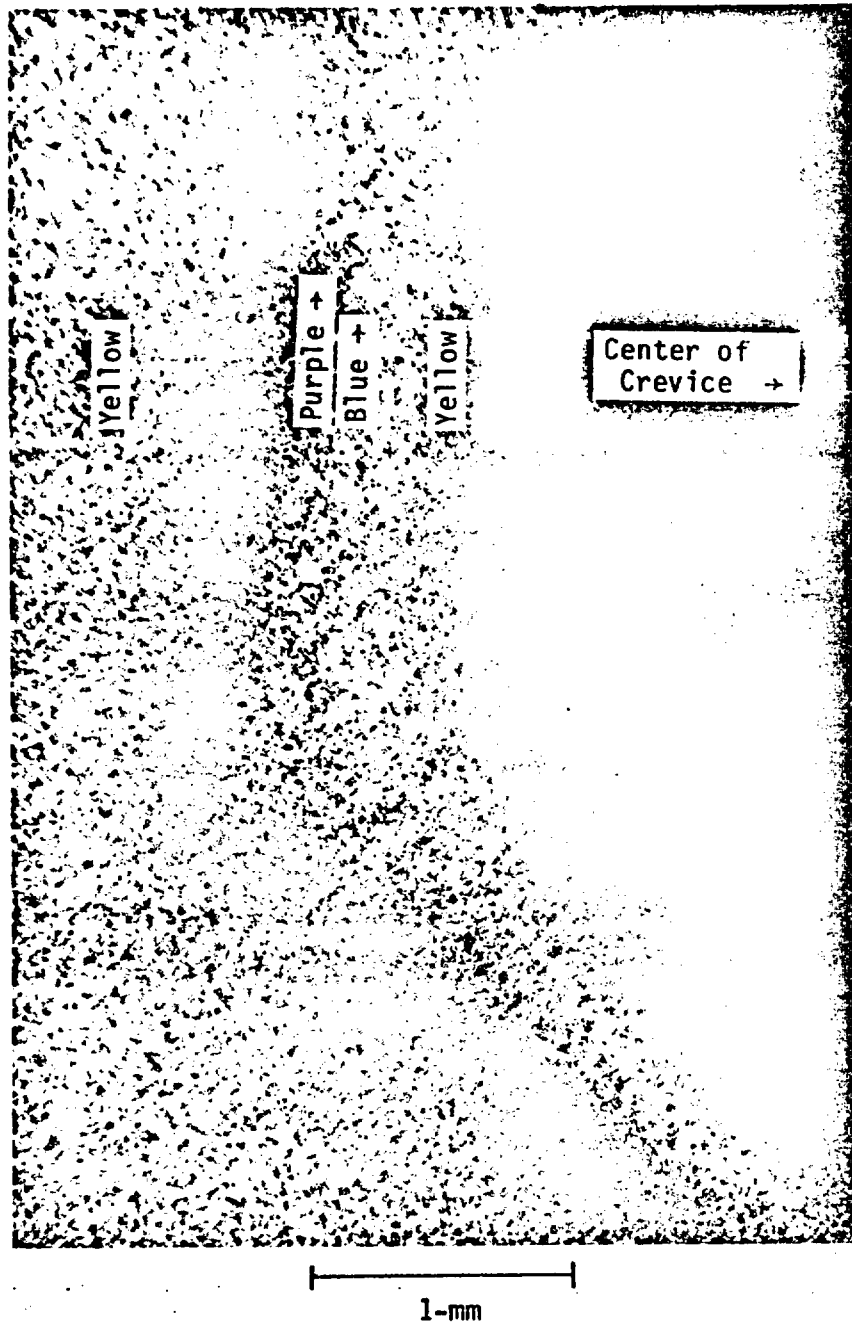


Figure 8. Corrosion product in the crevice of titanium.

of immersion did not give any consistent trend in weight change probably because of the inconsistent crevice clearance. TiCode-12 and EB TiCode-12 showed only slight color change in the crevice after two weeks at this temperature (Figure 9). However, at higher temperatures (200°C), the film was formed more easily.

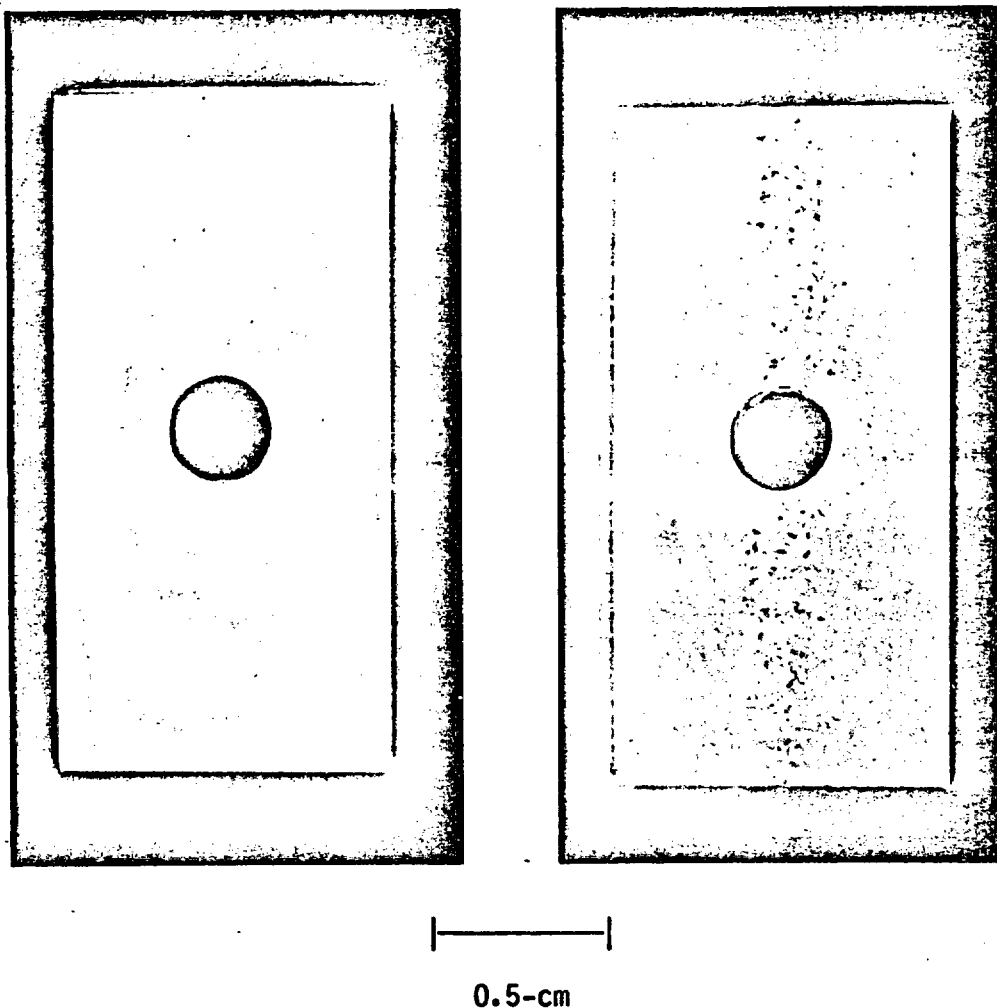
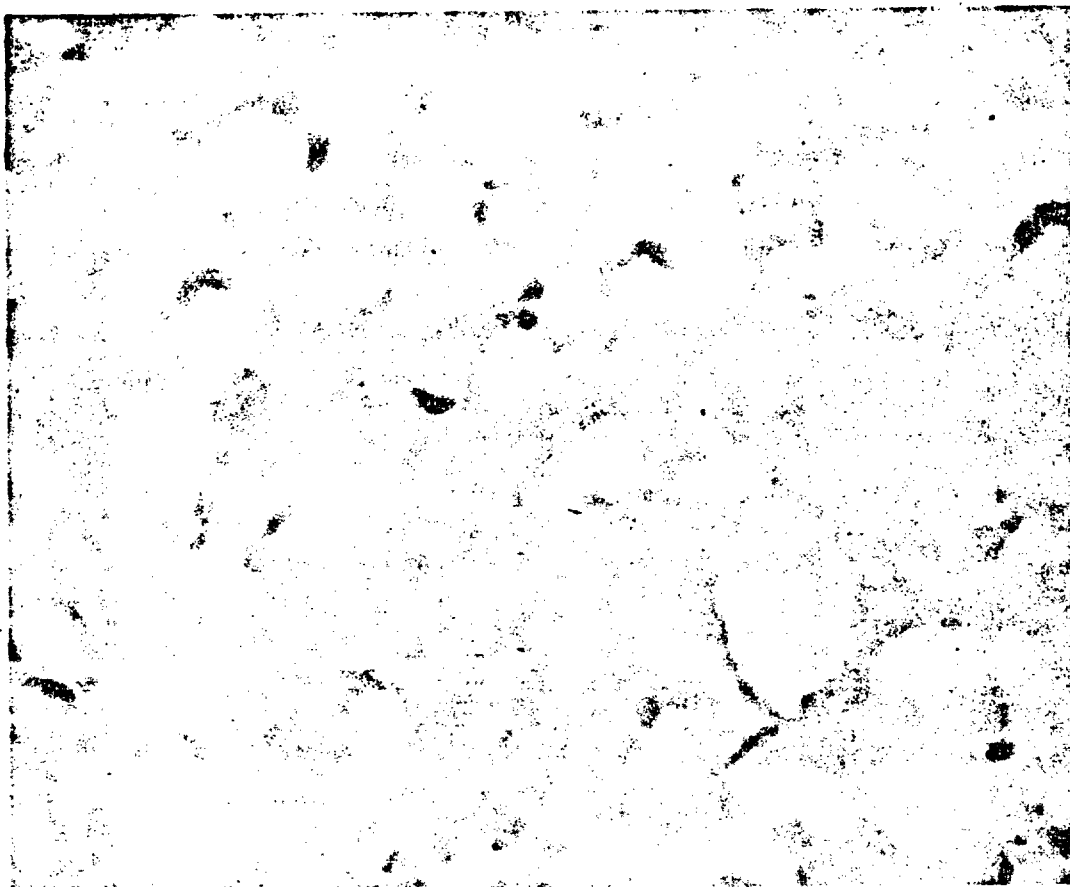


Figure 9. Corrosion product in the crevice of TiCode-12 and EB Ti-Code-12.

The film obtained in the crevice of titanium was removed by immersion in aqua regia for TEM observation. Aqua regia causes preferential dissolution of the matrix beneath the film. This film was found to be a combination of  $TiO_2$  and lower oxides such as  $Ti_2O_3$ ,  $TiO$  and  $Ti_3O_5$  (Figure 10). The possible existence of hydride was also noted. The modification of the oxides by Aqua Regia is under consideration. The film formed on TiCode-12 and EB TiCode-12 will be analyzed.

The existence of crevice corrosion in titanium is consistent with previous observations.<sup>2,14</sup> For titanium to undergo crevice corrosion the solution within the crevice must become and remain significantly acid. This is obtained by the establishment of macrocells upon the depletion of oxygen within the crevice with a decrease of corrosion potential.<sup>14</sup> Considering the high tem-



10  $\mu$

Figure 10. TEM microstructure of lower oxides in the crevice region for titanium.

perature potential-pH diagram,<sup>17</sup> the lower oxide formation suggests that acidification is in progress by the continuous depletion of oxygen in the crevice. The colored film may be lower oxides while the black film a hydride.<sup>16</sup> They would be formed by cathodic and various anodic reactions because of differing degrees of polarization obtained in the crevice region. An alternative interpretation of the existence of lower oxides is also possible. If indeed the crevice achieves an active or active-passive transition state the anodic product expected is a surface monolayer.<sup>16</sup> In this situation, the observed oxide may form from the interaction between the dissolved corrosion product and the external solution.

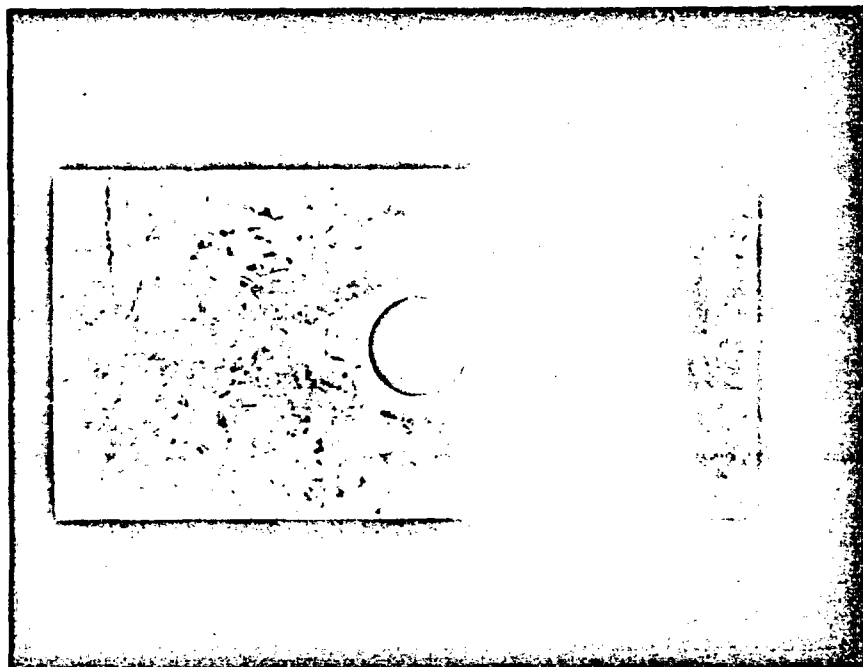
It is generally known that the presence of dilute alloying elements, Ni and Mo, as in TiCode-12, increases the uniform and crevice corrosion resistance<sup>4,14,18</sup> of titanium. However, the present findings on the color change at 150°C and film formation at 200°C implies that this alloy may not be completely immune to crevice corrosion under repository conditions. Previous experimental results<sup>14,18</sup> for Ti-Ni and Ti-Mo in an acidic environment and our electrochemistry results do not completely answer this question at the moment because of the lack of knowledge of real crevice environments. The confirmation of the degree of crevice corrosion susceptibility of TiCode-12 and EB TiCode-12 will be continued and the results will be interpreted in relation to the results of the electrochemical investigations.

Information on crevice corrosion in copper is very limited. The modified ASTM<sup>19</sup> method was used for crevice simulation by tightening two coupons with rubber bands with a Teflon tape providing clearance at one end. While Cu/Cu and Cu/Teflon interfaces showed no visible changes after 3 to 9 weeks, a major corrosion product (black) was apparent beneath the rubber band (Figure 11). EDAX analysis showed a sulfur peak from this product. One probable reason is the preferential attack by sulfur leached from the rubber bands. The reaction of copper with sulfide has been postulated previously in the use of copper as a container material since there are a number of sulfide sources in the waste repository including the buffered bed, groundwater or from bacterial action.<sup>5</sup>

#### 6. DETERMINATION OF POTENTIAL-pH DIAGRAMS FOR Cu, Pb, AND Ti IN AQUEOUS SOLUTIONS WITH HIGH CHLORIDE CONTENT.

Calculations have been made on the electrochemical corrosion of copper, lead, and titanium exposed to Brine A and B at 25°C. The ions which were considered to be the most important in causing corrosion are listed in Table 5. These activities do not correspond exactly to the concentration. However, the differences do not significantly affect the calculations. The values for the equilibrium constant for copper were obtained primarily from the Swedish report on copper as a container material.<sup>5</sup> The values for lead and titanium were calculated from free energy data.<sup>20</sup>

For titanium, the anhydrous state was considered. The potential-pH diagram was not altered significantly from the diagram of the system of titanium and pure water.<sup>21</sup> By considering the influence of the ions shown in Table 5, it was found that there are no stable chloro-complexes of titanium.



1-cm x 2-cm coupon

Figure 11. Sulfur attack on copper observed at the interface of Cu/rubber band.

Table 5

Ions Considered in the Potential-pH Diagram

Ions (moles/liter)	Cl <sup>-1</sup>	SO <sub>4</sub> <sup>-2</sup>	I <sup>-1</sup>	HCO <sub>3</sub> <sup>-1</sup>	H <sup>+1</sup>
Brine A	5.4	3.6x10 <sup>-4</sup>	7.9x10 <sup>-5</sup>	1.1x10 <sup>-2</sup>	3.2x10 <sup>-7</sup>
Brine B	4.9	3.6x10 <sup>-4</sup>	7.9x10 <sup>-4</sup>	1.6x10 <sup>-4</sup>	3.2x10 <sup>-7</sup>

For copper, however, new domains of Cu(OH)<sub>1.5</sub>Cl<sub>0.5</sub> and CuCl<sub>2</sub> are observed (Figure 12) than had been shown in the system of Cu-Cl-H<sub>2</sub>O (355 ppm Cl<sup>-</sup>).<sup>22</sup> As shown in the diagram, it is also probable for copper to dissolve to form aqueous chloro-complexes in the domain where copper is immune to corrosion in pure water.

In the case of lead as a radiation shielding material, the stability of PbSO<sub>4</sub> and PbCl<sub>2</sub> have been introduced (Figure 13) compared to their absence

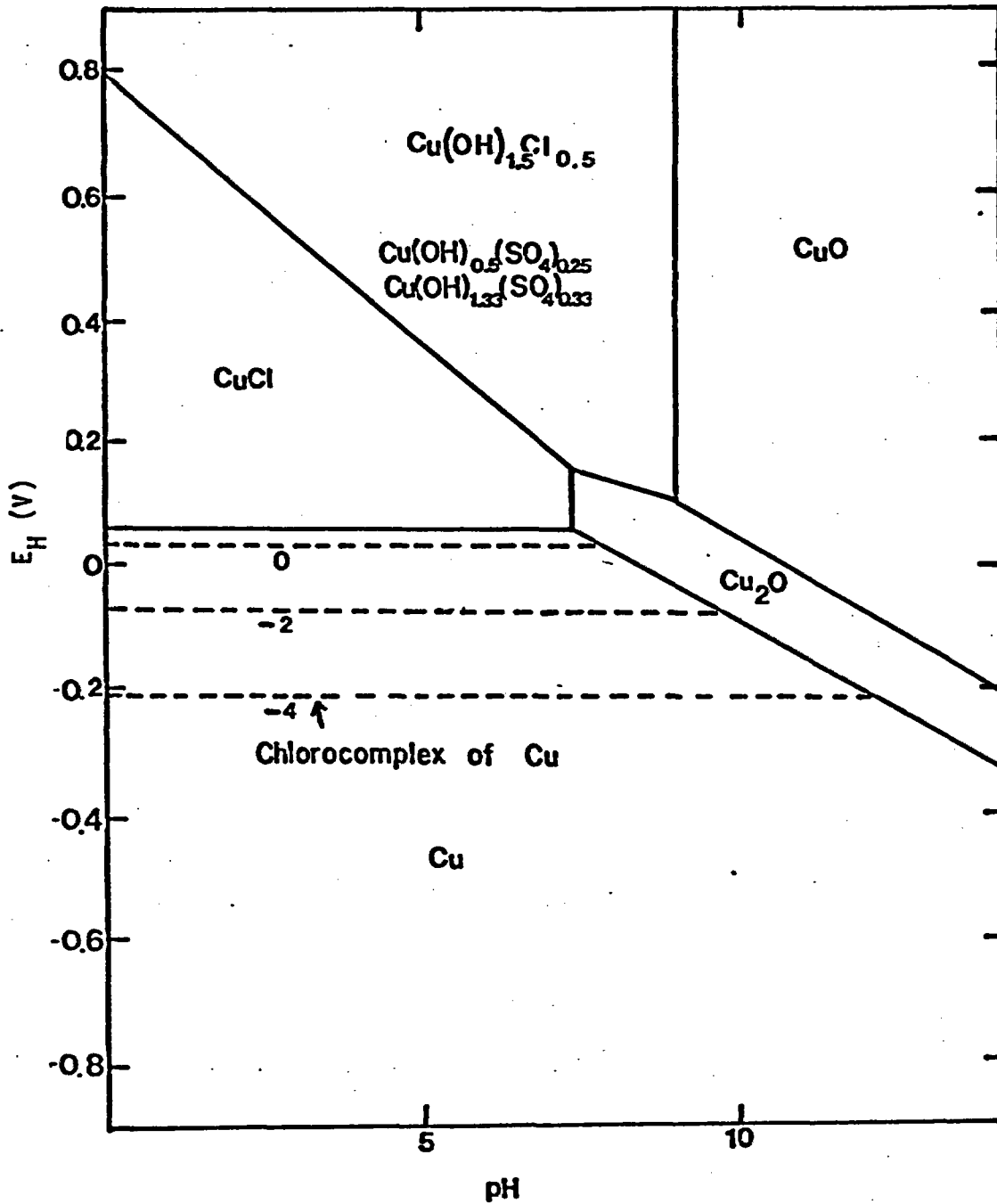


Figure 12. Potential-pH equilibrium diagram for the system Copper-Brine A and B at 25°C.

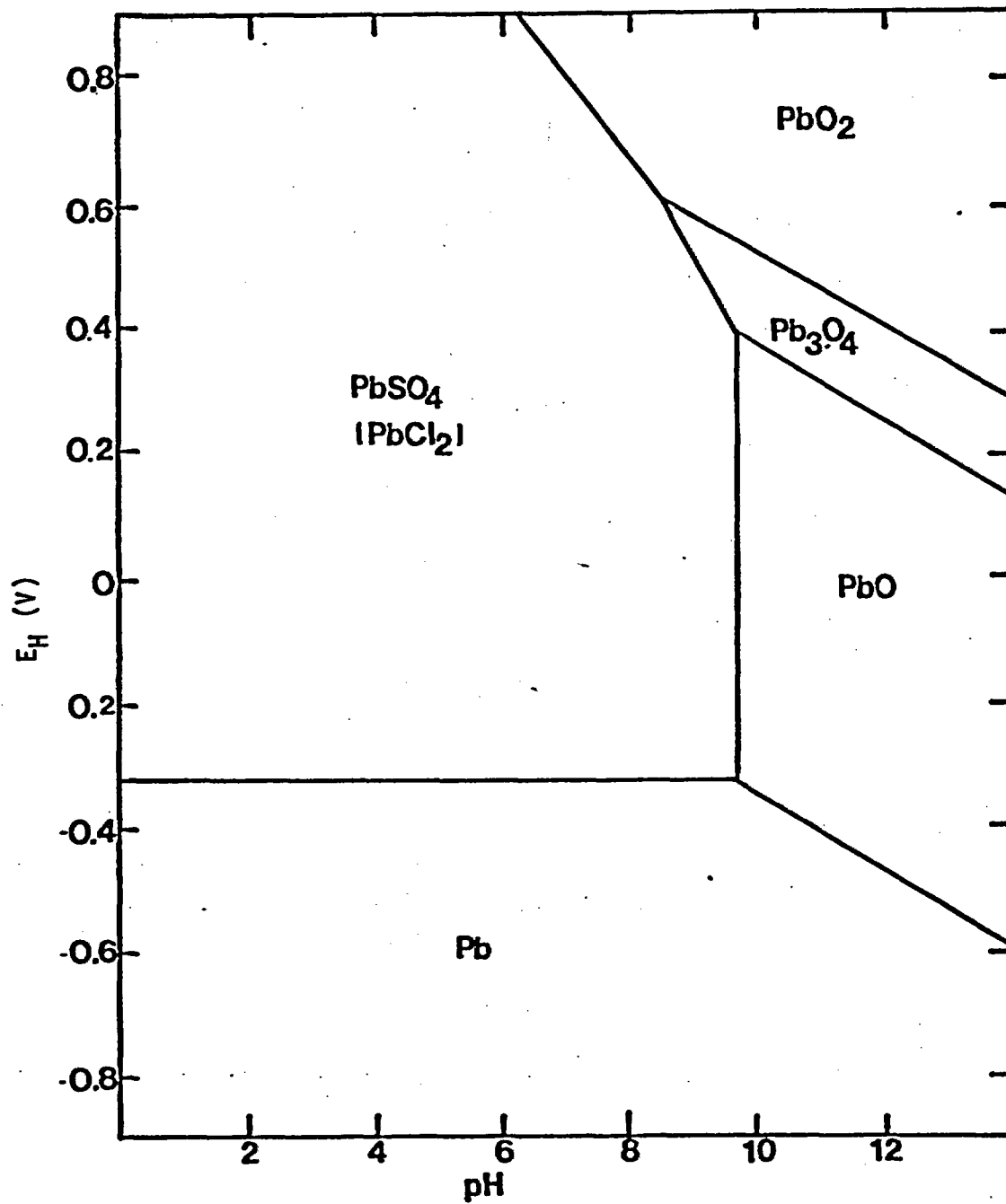


Figure 13. Potential-pH equilibrium diagram for the system Lead-Brine A and B in the absence of  $\text{HCO}_3^-$  at 25°C.

in the lead-pure water system.<sup>21</sup> The formation of this compound may affect the passivity of any solid film formed on this material.

The results obtained in this calculation are used for an understanding of uniform as well as localized corrosion of these materials. The work will be continued for higher temperatures.

## 7. STRESS CORROSION AND PITTING CORROSION

U-bend and C-ring specimens were designed following ASTM standards<sup>23,24</sup> as shown in Figure 14 for titanium. Part of the C-rings were precracked to provide stress concentration.<sup>25</sup> The stress levels of C-rings are being estimated.<sup>26</sup> Because it is difficult to detect stress corrosion susceptibility of TiCode-12 at 150°C in Brine A or B<sup>2</sup>, samples will be immersed in concentrated chloride solutions, such as LiCl<sup>27</sup>, in order to increase susceptibility. The components of the slow strain rate machine are in the laboratory being assembled. The ac Impedance and Scanning Reference Electrode Techniques are ready for pitting studies.

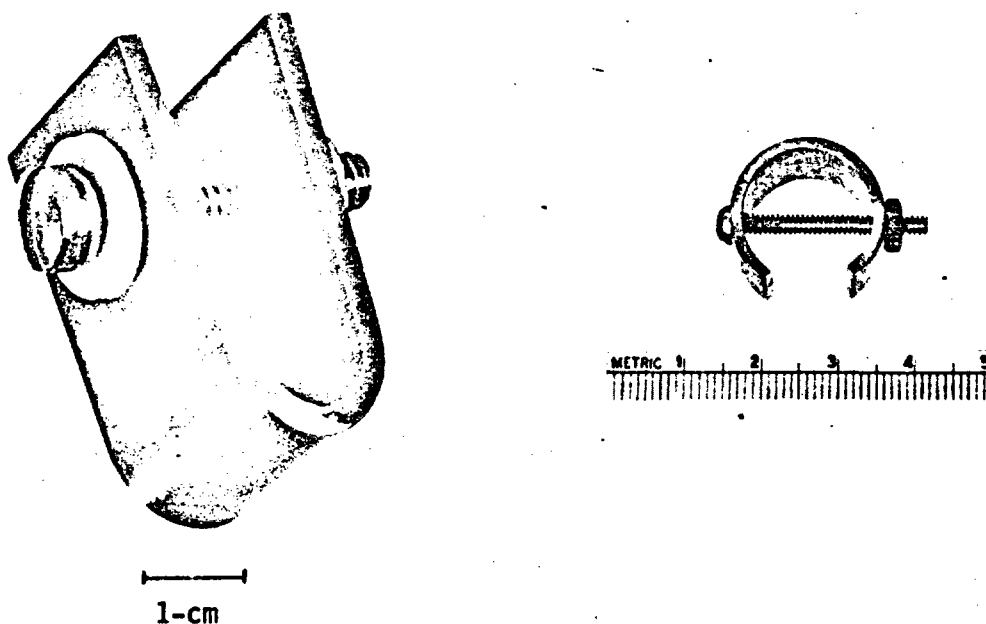


Figure 14. C-ring and U-bend specimens for stress corrosion testing.

## 8. HYDROGEN EMBRITTLEMENT

Effort has been made in setting up equipment for hydrogen analysis, and initial work in tensile and buckling testing has been performed in cathodically charged titanium and TiCode-12 in order to investigate the susceptibility of TiCode-12 to hydrogen embrittlement.

A method of hydrogen analysis is ready using a hot vacuum extraction procedure and a mass spectrometer. The pressure change and fraction of hydrogen present are determined. Typical heating conditions are 90°C and one hour for a coupon of 1-cm x 2-cm (0.5 - 1.0-mm) thickness. This facility will be used for hydrogen analysis in the case of possible hydrogen uptake during radiolysis and stress corrosion cracking where hydrogen embrittlement is expected to be the rate controlling factor.

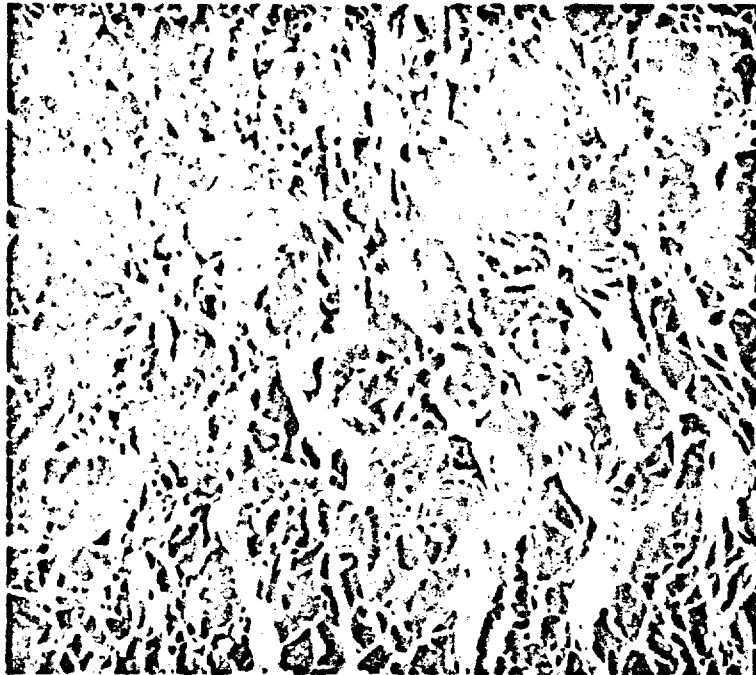
The tensile specimens of gauge length 2.54-cm were machined from sheet samples with a thickness of 0.5-mm for titanium and 0.9-mm for TiCode-12 in accordance with ASTM specifications.<sup>28</sup> These samples were hydrogenated cathodically in 10% sulfuric acid with  $3.1 \times 10^{-3}$  M  $\text{Na}_4\text{P}_2\text{O}_7$  cathodic poison for half to one hour at 90°C and 15 mA/cm<sup>2</sup>. Titanium was homogenized in argon at 500°C for one hour. Due to severe loss of hydrogen during homogenization, and the enhanced solubility<sup>29</sup> and diffusivity<sup>30</sup> of hydrogen in the presence of the beta phase, TiCode-12 was not homogenized.

Tensile testing was performed at a crosshead speed 0.05 mm/min (equivalent to an approximate strain rate  $2.5 \times 10^{-5}$ /sec) as a slow strain rate and 2.54 cm/min (equivalent to an approximate strain rate  $1.2 \times 10^{-2}$ /sec) as a high strain rate. As a reference, tensile specimens without hydrogenation were heat treated in the argon environment.

With titanium there was no significant change between charged and uncharged specimens in tensile strength, elongation, reduction area and fracture stress at high strain rate within experimental error. At the slow strain rate, however, the fracture stress was reduced by more than 20% while the changes in the other properties were not discernible. This result indicates that the hydrogen level was probably in the range of slow strain rate embrittlement, which is lower than the hydrogen content required for impact embrittlement.<sup>31</sup> This is consistent with previous observations that tensile properties are unaffected by a modest hydrogen addition<sup>32</sup> and that hydrogen content has a much more striking effect on fracture properties.<sup>33</sup>

For TiCode-12, the hydrogenated sample showed more than 30% decrease in elongation at the slow strain rate. Figure 15 shows embrittlement of features in a hydrogenated specimen in contrast to the ductile features of a nonhydrogenated specimen (Figure 16). This seems to be consistent with previous results on other alpha and beta titanium alloys<sup>34</sup> and the result of stress corrosion cracking under strongly cathodic conditions in TiCode-12.<sup>4</sup> No change of fracture stress seems to arise from the alteration of initial microstructure of nonhydrogenated samples by argon atmosphere heat treatment.<sup>35</sup> The slow strain rate sensitivity test on hydrogenated TiCode-12 will be repeated to confirm the present finding with extensive metallographic examination since slow strain rate embrittlement may be a major cause of delayed failure over extended times.

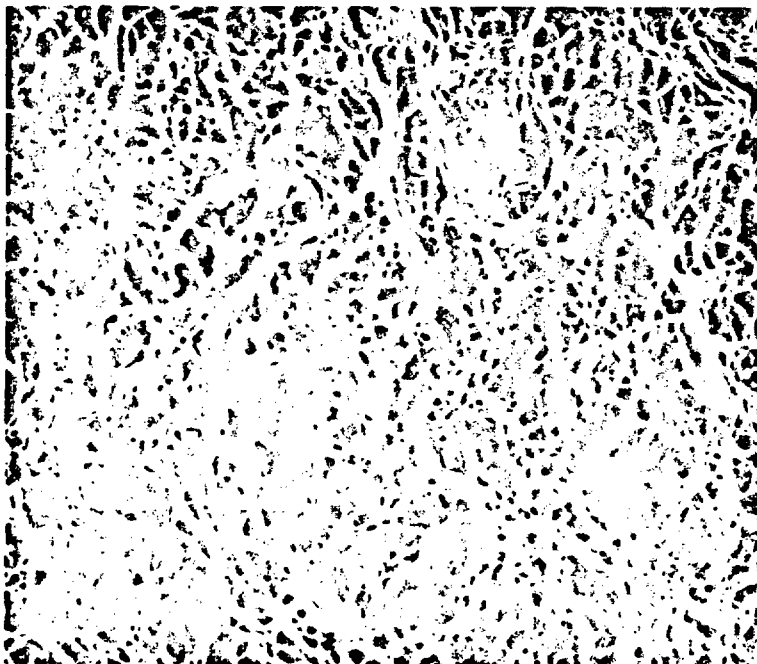
Impact embrittlement was found in a separate experiment using TiCode-12. Samples were cathodically charged in molten salt for two hours at 100 mA/cm<sup>2</sup>



↑  
heavily hydrogenated region

10  $\mu$

Figure 15. Fractograph of slow strain rate embrittled TiCode-12.



10  $\mu$

Figure 16. Fractograph of nonhydrogenated TiCode-12.

and 230°C. This method of charging allows larger amounts of hydrogen to be absorbed than by using aqueous solutions at atmospheric pressure. The hydrogenated sample fractured upon buckling while the nonhydrogenated sample did not (Figure 17). The subsequent microstructure confirmed this embrittlement effect (Figure 18).

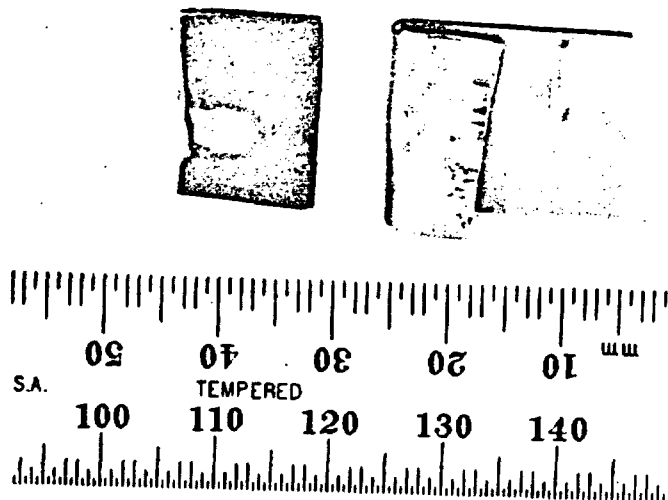
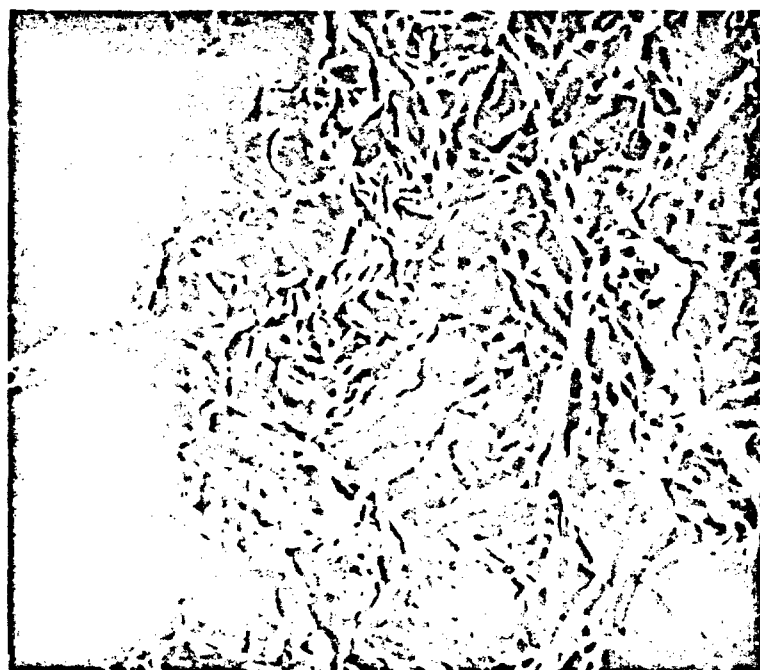


Figure 17. Buckling test result on hydrogenated and nonhydrogenated TiCode-12.



↑  
heavily hydrogenated region

—  
10 μ

Figure 18. Fractograph of impact embrittled TiCode-12.

## 9. RADIATION EFFECTS

Gamma radiolysis of brine solution is expected to produce oxidants as well as hydrogen, which influence the corrosion and hydrogen behavior of the materials being studied.<sup>4</sup> The principal species of interest are H<sub>2</sub>, O<sub>2</sub>, Cl<sub>2</sub>, H<sub>2</sub>O<sub>2</sub>, ClO<sub>3</sub>, ClO<sub>4</sub>, HNO<sub>3</sub>, and H<sub>2</sub>SO<sub>4</sub>. In this quarter, the effort was directed at setting up an irradiation cell in the gamma pool.

The irradiation cell used consisted of a 22.9-cm long 1.9-cm O.D. stainless steel tube with a 0.2-cm wall thickness. The bottom of the tube was welded shut and the top fitted with a Swagelok connector. Stainless steel tubing (0.6-cm O.D.) coupled to this connector was terminated in a manifold incorporating a rupture disc, gas handling valve and a strain gauge pressure transducer. 5-10 ml brine is irradiated in a silica liner tube at pool temperature (≈35°C) and atmospheric pressure. The pressure changes in the cell were recorded during irradiation to 10<sup>7</sup> and 10<sup>8</sup> rads, at a dose rate of  $\sim 4 \times 10^6$  rads/hour. Following irradiation, gas samples were analyzed in a mass spectrometer. Development of a suitable analytical technique for the analysis of irradiated brine is an ongoing task.

## 10. REFERENCES

1. R. E. Westerman, "Investigation of Metallic, Ceramic, and Polymeric Materials for Engineered Barrier Applications in Nuclear-Waste Packages", PNL-3484, Pacific Northwest Laboratory Report (1980).
2. J. W. Braithwaite, N. J. Magnani, and J. W. Munford, "Titanium Alloy Corrosion in Nuclear Waste Environments", Sandia Laboratory Report, SAND 79-2023C (1979).
3. J. W. Braithwaite and N. J. Magnani, "Nuclear Waste Canister Corrosion Studies Pertinent to Geologic Isolation", Nuclear and Chemical Waste Management 1, 37 (1980).
4. M. A. Molecke, D. W. Schaefer, R. S. Glass, and J. A. Ruppen, "Sandia HLW Canister/Overpack Studies Applicable for a Salt Repository", Sandia Laboratory Report, SAND 81-1585 (1981).
5. "Copper as Canister Material for Unreprocessed Nuclear Waste--Evaluation with Respect to Corrosion", Swedish KBS Technical Report 90 (1978).
6. "Lead-Lined Titanium Canisters for Reprocessed and Vitrified Nuclear Fuel Waste, Evaluation of the Corrosion Aspects", Swedish KBS Technical Report 107 (1978).
7. S. Henrikson and M. de Pourbaix, "Corrosion Testing of Unalloyed Titanium in Simulated Disposal Environments for Reprocessed Nuclear Waste", Swedish KBS Technical Report 96 (1978).
8. T. M. Ahn, B. S. Lee, and P. Soo, "Container Assessment - Corrosion Study of HLW Container Materials", Quarterly Progress Report, April-June 1981, Brookhaven National Laboratory Report, BNL-NUREG-51449 (1981).
9. T. E. Scott, "Issues Relevant to Nuclear Waste Canister Materials", in Corrosion/80, NACE, Paper #210, Proc. of Conference held March 1980, Chicago, IL.
10. "Standard Recommended Practice for Laboratory Immersion Corrosion Testing of Metals", ASTM Designation G31-72, Annual Book of ASTM Standards, Part 10, Metals - Physical, Mechanical Corrosion Testing, (1979).
11. C. O. Buckwalter, paper presented on the specific ion effect on waste form leaching in MCC workshop on the leaching mechanisms of nuclear waste forms, Battelle Seattle Research Center, October (1981).
12. R. Dayal, B. S. Lee, R. Wilke, K. J. Swyler, P. Soo, T. M. Ahn, N. S. McIntyre, and E. Veakis, NRC Nuclear Waste Management Technical Support in the Development of Nuclear Waste Form Criteria, BNL Informal Report, BNL-NUREG-27961R (1981).

13. F. A. Posey and E. G. Bohlmann, "Pitting of Titanium Alloys in Saline Water", *Desalination* 3, 269 (1967).
14. J. C. Griess, Jr., "Crevice Corrosion of Titanium in Aqueous Salt Solutions", *Corrosion-NACE* 24, 96 (1968).
15. G. T. Burstein and R. C. Newman, *Electrochim. Acta* 25, 1009 (1980).
16. E. J. Kelly, "Anodic Dissolution and Passivation of Titanium in Acidic Media III Chloride Solutions", *J. Electrochem. Soc.* 126, 2064 (1979).
17. D. D. MacDonald, B. C. Syrett, and S. S. Wing, "The Use of Potential-pH Diagrams for the Interpretation of Corrosion Phenomena in High Salinity Geothermal Brines", *Corrosion* 35, 1 (1979).
18. N. D. Tomashov, G. P. Chernova, Y. S. Ruscol, and jG. A. Aynyan, "The Passivation of Alloys on Titanium Bases", *Electrochemica Acta* 19, 159 (1974).
19. "Standard Test Methods for Pitting and Crevice Corrosion Resistance of Stainless Steels and related Alloys by the Use of Ferric Chloride Solution", ASTM G48-76, *ibid.* reference 10.
20. *Handbook of Chemistry and Physics*, 56th Edition, CRC Press (1976).
21. M. Pourbaix, *Atlas of Electrochemical Equilibria in Aqueous Solutions*, NACE (1974).
22. M. Pourbaix, "Some Applications of Potential-pH Diagrams to the Study of Localized Corrosion", *J. Electrochem. Soc.* 123, 250 (1976).
23. "Standard Recommended Practice for Making and Using U-bend Stress Corrosion Test Specimens", ASTM G30-72, *ibid.* reference 10.
24. "Standard Recommended Practice for Making and Using C-ring Stress Corrosion Test Specimens", ASTM G38-73, *ibid.* reference 10.
25. E. J. Jankowsky, "Notched C-ring Test", p. 51, in Hydrogen Embrittlement Testing, ASTM (1972).
26. S. O. Fernandez and G. F. Tisinai, "Stress Analysis of Unnotched C-rings Used for Stress Cracking Studies", *J. of Engineering for Industry*, 47 (1968).
27. M. J. Blackburn and W. H. Smyrl, "Stress Corrosion and Hydrogen Embrittlement", p. 2577, in Titanium Science and Technology, edited by R. I. Jaffee and H. M. Burte, AIME (1972).
28. "Standard Methods of Tension Testing of Metallic Materials", ASTM E8-79, *ibid.* reference 10.

29. N. E. Paton and J. C. Williams, "Effects of Hydrogen on Titanium and its Alloys", p. 409, in Hydrogen in Metal, edited by ASM (1973).
20. R. J. Wasilewski and G. L. Kehl, "Diffusion of Hydrogen in Titanium" Metallurgica, 225 (1954).
31. D. N. Williams, "The Hydrogen Embrittlement of Titanium Alloys", p. 185, in Hydrogen Damage, edited by C. D. Beachem, ASM (1979).
32. K. J. Puttlitz and A. J. Smith, "Embrittlement of Pure and Commercially Pure Titanium", p. 427, in Hydrogen Effects in Metals, edited by I. M. Bernstein and A. W. Thompson, AIMI (1980).
33. D. N. Williams, "Effects of Hydrogen in Titanium Alloys on Subcritical Crack Growth under Sustained Load", Materials Science and Engineering **24**, 531 (1976).
34. G. A. Lenning, C. M. Craighead, and R. I. Jaffee, "Constitution and Mechanical Properties of Titanium-Hydrogen Alloys", p. 100, *ibid.* reference 31.
35. G. T. Terlinde, T. W. Dueriq, and J. C. Williams, "The Effect of Heat Treatment on Microstructure and Tensile Properties of Ti-10V-2Fe-2Al", in Titanium '80, p. 1571, edited by H. Kimura and O. Izumi (1980).